




# RTL8 promotes nuclear localization of UBQLN2 to subnuclear compartments associated with protein quality control

Harihar Milaganur Mohan<sup>1,2</sup> · Hanna Trzeciakiewicz<sup>1</sup> · Amit Pithadia<sup>1</sup> · Emily V. Crowley<sup>1</sup> · Regina Pacitto<sup>1</sup> · Nathaniel Safren<sup>1,3</sup> · Bryce Trotter<sup>1</sup> · Chengxin Zhang<sup>4</sup> · Xiaogen Zhou<sup>4</sup> · Yang Zhang<sup>4</sup> · Venkatesha Basrur<sup>5</sup> · Henry L. Paulson<sup>1,6</sup> · Lisa M. Sharkey<sup>1,6</sup> 

Received: 19 April 2021 / Revised: 17 January 2022 / Accepted: 25 January 2022 / Published online: 5 March 2022  
© The Author(s), under exclusive licence to Springer Nature Switzerland AG 2022

## Abstract

The brain-expressed ubiquilins (UBQLNs) 1, 2 and 4 are a family of ubiquitin adaptor proteins that participate broadly in protein quality control (PQC) pathways, including the ubiquitin proteasome system (UPS). One family member, UBQLN2, has been implicated in numerous neurodegenerative diseases including ALS/FTD. UBQLN2 typically resides in the cytoplasm but in disease can translocate to the nucleus, as in Huntington's disease where it promotes the clearance of mutant Huntingtin. How UBQLN2 translocates to the nucleus and clears aberrant nuclear proteins, however, is not well understood. In a mass spectrometry screen to discover UBQLN2 interactors, we identified a family of small (13 kDa), highly homologous uncharacterized proteins, RTL8, and confirmed the interaction between UBQLN2 and RTL8 both in vitro using recombinant proteins and in vivo using mouse brain tissue. Under endogenous and overexpressed conditions, RTL8 localizes to nucleoli. When co-expressed with UBQLN2, RTL8 promotes nuclear translocation of UBQLN2. RTL8 also facilitates UBQLN2's nuclear translocation during heat shock. UBQLN2 and RTL8 colocalize within ubiquitin-enriched subnuclear structures containing PQC components. The robust effect of RTL8 on the nuclear translocation and subnuclear localization of UBQLN2 does not extend to the other brain-expressed ubiquilins, UBQLN1 and UBQLN4. Moreover, compared to UBQLN1 and UBQLN4, UBQLN2 preferentially stabilizes RTL8 levels in human cell lines and in mouse brain, supporting functional heterogeneity among UBQLNs. As a novel UBQLN2 interactor that recruits UBQLN2 to specific nuclear compartments, RTL8 may regulate UBQLN2 function in nuclear protein quality control.

**Keywords** Ubiquilin · UBQLN2 · RTL8 · Nuclear protein quality control · Ubiquitin proteasome system

✉ Henry L. Paulson  
henryp@med.umich.edu

✉ Lisa M. Sharkey  
lisams@med.umich.edu

<sup>1</sup> Department of Neurology, University of Michigan, Ann Arbor, MI 48109-2200, USA

<sup>2</sup> Graduate Program in Cellular and Molecular Biology, University of Michigan, Ann Arbor, MI 48109-2200, USA

<sup>3</sup> Present Address: Department of Neurology, Northwestern University Feinberg School of Medicine, Chicago, IL 60611, USA

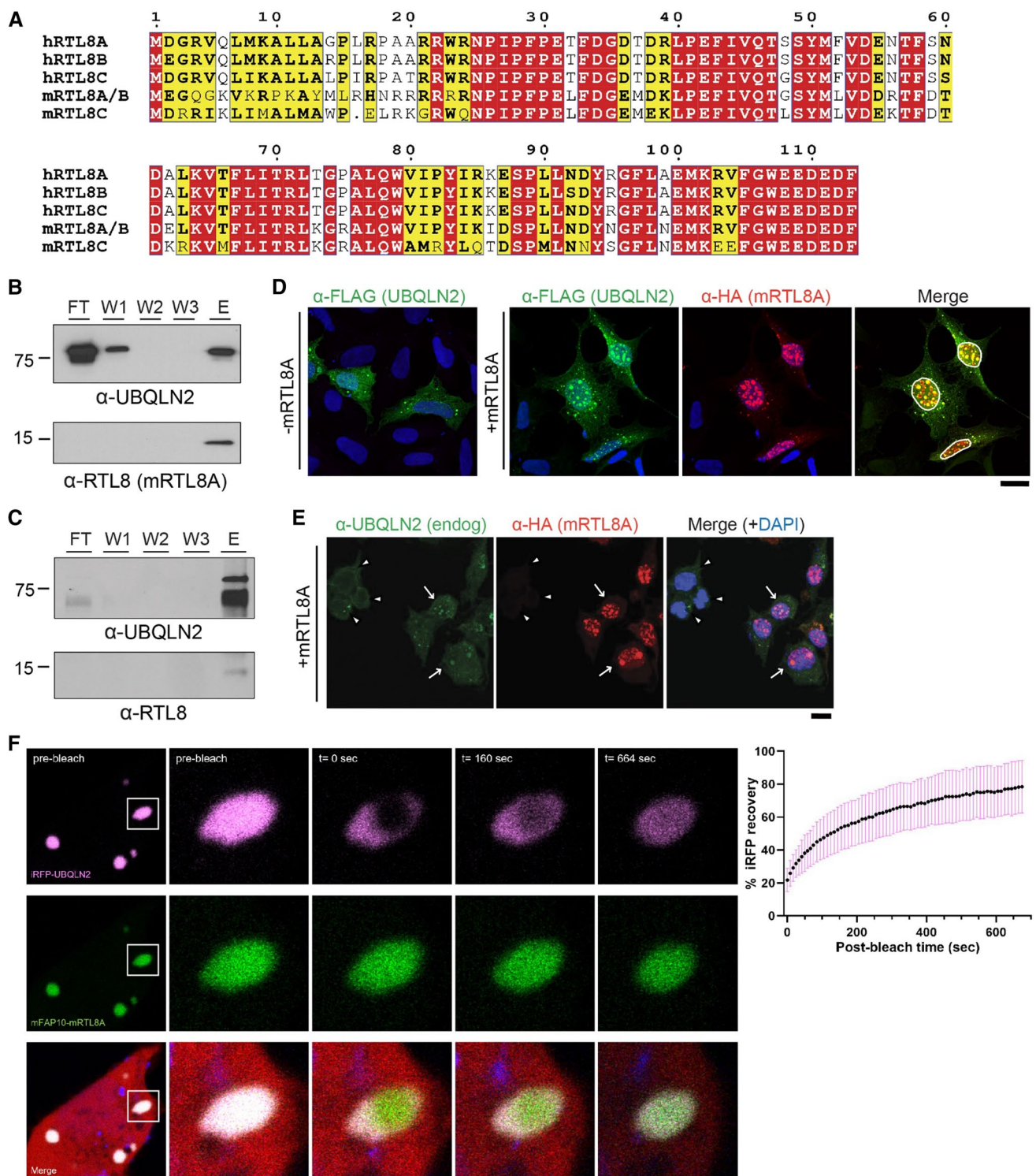
<sup>4</sup> Department of Computational Medicine and Bioinformatics, University of Michigan, Ann Arbor, MI 48109-2200, USA

<sup>5</sup> Department of Pathology, University of Michigan Medical School, Ann Arbor, MI 48109, USA

<sup>6</sup> Michigan Neuroscience Institute, University of Michigan, Ann Arbor, MI 48109-2200, USA

## Introduction

UBQLN2 is a member of the ubiquilin family of proteins that participate in ubiquitin-dependent protein quality control (PQC) pathways [1–3]. While UBQLN2 is best known as a shuttle adaptor protein for the ubiquitin–proteasome system (UPS), it is also implicated in autophagy, stress granule dynamics and chaperone-dependent pathways [4–7]. This versatility reflects various functional domains in UBQLN2, including its ubiquitin-binding (UBA) and ubiquitin-like (UBL) domains, as well as its propensity to engage in liquid–liquid phase separation (LLPS) [3, 8–10]. Wild-type UBQLN2 accumulates in numerous neurodegenerative diseases including Huntington's disease (HD), Lewy body dementia and amyotrophic lateral sclerosis (ALS)/frontotemporal dementia (FTD) caused by the *C9ORF72* repeat expansion [11–15]. When mutated, UBQLN2 directly



causes hereditary neurodegeneration that manifests as ALS/FTD spectrum disease associated with UBQLN2 and TDP-43 accumulation [16–18]. Multiple animal models with UBQLN2 mutations found in human disease partially phenocopy human pathology, providing useful tools to study the molecular mechanisms of disease [17, 19–22].

Precisely how UBQLN2 functions in PQC pathways is not well understood, nor is it clear how UBQLN2 mutations drive neurodegeneration. In both cases, however, UBQLN2 protein–protein interactions appear to play a critical role. For example, UBQLN2 missense mutations have been shown to compromise UBQLN2 function in

**Fig. 1** RTL8, a family of small UBQLN2 interacting proteins, promotes nuclear translocation of UBQLN2. **A** Alignment of the protein sequences for the human (hRTL8) and murine (mRTL8) RTL8 proteins, showing a high degree of sequence homology. Similar residues are boxed in yellow; the bold typeface indicates that these residues are found in the majority of RTL8 homologs. Identical residues are bolded in white font and boxed in red. **B** Immunoblots of *in vitro* pull-down of recombinant purified protein GST-UBQLN2 and His-mRTL8A.  $\alpha$ -UBQLN2 and  $\alpha$ -RTL8 antibodies were used for immunoblotting. UBQLN2-mRTL8A interaction was confirmed by detection of mRTL8A in the eluate (E), flow-through (FT), and washes (W1-3) as shown. **C** Immunoprecipitated FLAG-UBQLN2 pull down of RTL8 from brain lysates of FLAG-tagged UBQLN2 transgenic mice. **D** Representative images showing mRTL8A-dependent nuclear translocation of UBQLN2 and co-localization into subnuclear puncta. HEK293 cells were co-transfected with FLAG-UBQLN2 (green) and control HA-empty vector or HA-mRTL8A (left panel and right series, respectively). DAPI (blue) stained nuclei. White outlines in the merged image mark nuclei (scale bar = 20  $\mu$ m). **E** Representative images showing mRTL8A-mediated nuclear translocation of endogenous (endog) UBQLN2. HEK293 cells were transfected with HA-mRTL8A and stained for endogenous UBQLN2 (green) and HA-mRTL8A (red). Merged images include DAPI to highlight nuclei (blue). Arrows highlight cells demonstrating localization of endogenous UBQLN2 to nuclear puncta containing HA-mRTL8A. Arrowheads identify cells not expressing HA-mRTL8A in which UBQLN2 is diffusely cytoplasmic (scale bar = 10  $\mu$ m). **F** Representative images showing fluorescence recovery after photobleaching (FRAP) of UBQLN2-mRTL8A puncta, demonstrating their dynamic nature. HEK293 cells were transfected with iRFP-UBQLN2 (pink), mFAP10-mRTL8A (green) and mApple (red). mApple serves as a morphology marker (scale bar = 5  $\mu$ m). (Right) iRFP fluorescence recovery following bleach was plotted as a percentage of the average fluorescence intensity of the puncta over time. Data are shown as mean  $\pm$  SD.  $N = 17$  puncta

PQC by reducing interactions with Hsp70, limiting delivery of polyubiquitinated proteins to the proteasome, reducing autophagy, and altering liquid–liquid phase separation (LLPS) in a manner that promotes UBQLN2 accumulation and aggregation [9, 16, 19, 22–27].

Here we sought to identify novel UBQLN2 interactors because greater knowledge of the range of UBQLN2 protein interactors will aid our understanding of how UBQLN2 acts, both in health and disease. Knowledge of the UBQLN2 interactome could also help explain why UBQLN2, principally a cytoplasmic PQC factor, translocates to the nucleus under proteotoxic stress [19]. For example, in HD mouse models, UBQLN2 localizes to neuronal nuclei where it is thought to facilitate clearance of mutant Huntingtin [13–15, 28]. Several membraneless organelles in the nucleus, notably nucleoli and PML bodies, have recently been implicated in nuclear PQC [29, 30]. These subnuclear condensates undergo phase transitions from liquid-like to solid states to sequester stress-induced misfolded and aggregated proteins [29–32]. UBQLN2 is already known to regulate the dynamics of stress granules [7], which are cytosolic condensates that modulate protein translation under conditions of stress.

Conceivably, UBQLN2 plays a similar role in regulating nuclear condensates.

Here we report a novel UBQLN2 interactor, RTL8 (previously known as FAM127 or CXX1), that readily localizes to the nucleus, regulates the subcellular localization of UBQLN2, and colocalizes with UBQLN2 in subnuclear condensates. RTL8 belongs to a family of neo-functionalized retrotransposon-derived Gag-like genes that include three highly homologous proteins, RTL8A, RTL8B and RTL8C. RTL8 proteins are largely unstudied. While no function has been ascribed to the RTL8 family, they are expressed throughout the body and in a wide range of human tumors [33–35]. Recently Whiteley and colleagues [36] identified RTL8 as one of several proteins whose levels are dysregulated in UBQLN2 murine disease and knockout models, consistent with our finding that RTL8 is a UBQLN2-interacting protein. Here we show that upon overexpression, RTL8 promotes UBQLN2 localization to the nucleus. At endogenous levels, RTL8 is critical for the efficient translocation of UBQLN2 to the nucleus under heat shock. We demonstrate that both proteins localize to subnuclear puncta that contain additional PQC components and are often adjacent to PML bodies. We also find that while UBQLN2's ubiquitin-binding (UBA) domain is not required for its interaction with RTL8, it is important for its incorporation into subnuclear puncta. Moreover, RTL8 preferentially colocalizes with and promotes the nuclear localization of UBQLN2 over the two other brain-expressed ubiquilin proteins, UBQLN1 and UBQLN4. UBQLN2—more than UBQLN1 and UBQLN4—also stabilizes RTL8 levels in cells and mouse brains, pointing to functional differences among ubiquilins.

## Results

### UBQLN2 interacts with a small nuclear protein, RTL8C, that promotes UBQLN2 translocation into the nucleus

To identify novel UBQLN2-interacting proteins we performed an unbiased mass spectrometry (MS) immunoprecipitation screen using HEK293T cells transfected with FLAG-tagged WT-UBQLN2 (FLAG-UBQLN2). Repeated MS experiments detected many previously identified UBQLN2 interactors including proteasome subunits, chaperones, and other UBQLN family members, supporting the robustness of our MS assay (Supplementary Table 1). Among abundant interactors, we detected a 13 kDa protein, retrotransposon Gag-like protein 8C (RTL8C) (Fig. S1A). Human RTL8C (hRTL8C) is one of three members of the RTL8 family of retrotransposon-derived proteins conserved between mouse and humans, the others being RTL8A and RTL8B (Fig. 1A). Human RTL8 proteins are more than 90% homologous (Fig.



S1B). Indeed, RTL8C was identified by a total of six peptides, two of which were unique to it while the other four are shared with RTL8A, leaving open the possibility that UBQLN2 interacts with more than one member of the RTL8 family. For clarity, we use the terminology RTL8 to refer to the family of proteins when antibodies are unable to differentiate them in our experiments.

We predicted a structure model for hRTL8C using C-I-TASSER [37] and deposited it in the neXtProt database [38] at [https://www.nextprot.org/entry/NX\\_A6ZKI3/gh/zhanglabs/COFACTOR](https://www.nextprot.org/entry/NX_A6ZKI3/gh/zhanglabs/COFACTOR). The predicted hRTL8C monomeric structure consists mainly of four alpha helical and loop domains (Fig. S1C) with an estimated TM-score of 0.65 (a TM-score > 0.5 suggests correct global topology [39]). This predicted structure displays homology with the capsid protein of the related retrotransposon Ty3/Gypsy [34] and *Drosophila melanogaster* retrovirus-like Arc1 protein [40].

To enable further *in vitro* and *in vivo* experiments, we cloned the mouse RTL8A gene (mRTL8A) which is the mouse RTL8 family member most similar to hRTL8C (Fig. S1B). To confirm a direct interaction between mRTL8A and UBQLN2, we performed pull-down experiments with recombinant GST-tagged UBQLN2 and His-tagged mRTL8A. GST-UBQLN2 purified protein was applied to a GST agarose column to which His-mRTL8A was then added. When reduced glutathione was used to elute UBQLN2, immunoblot analysis revealed mRTL8A in the eluate, confirming a direct interaction between the two proteins (Fig. 1B). The finding of a direct interaction is supported by previous observations from other groups [36].

Confirmation of interaction between UBQLN2 and endogenous RTL8 was obtained in mouse brain by immunoprecipitating FLAG-UBQLN2 from transgenic mice expressing a low level of wild-type (WT) FLAG-UBQLN2 [25]. Mouse brain lysate from UBQLN2 transgenic mice was incubated with anti-FLAG agarose beads and, after washing, FLAG-UBQLN2 was eluted from the beads. Immunoblot analysis demonstrated the presence of RTL8 in the eluate (Fig. 1C), confirming an *in vivo* interaction between the two proteins in brain.

To determine whether UBQLN2 and mRTL8A interact and co-localize *in vivo*, HEK293 cells were co-transfected with FLAG-UBQLN2 and HA-tagged mRTL8A (HA-mRTL8A). Expressed alone, FLAG-UBQLN2 was found diffusely and in small puncta in the cytoplasm (Fig. 1D, left panel) as described previously [19, 25]. When co-transfected with HA-mRTL8A, however, FLAG-UBQLN2 translocated into the nucleus where it co-localized with mRTL8A (Fig. 1D, right panel). HEK293 cells transfected with HA-mRTL8A alone recruited endogenous UBQLN2 into the nucleus (Fig. 1E, white arrows), whereas endogenous UBQLN2 remained largely cytoplasmic in untransfected cells (Fig. 1E, white arrowheads). We verified that

human RTL8C (hRTL8C) showed a similar staining pattern with overexpressed UBQLN2 as observed with mRTL8A. hRTL8C expressed alone localized to the nucleus, similar to mRTL8A (Figure S1D). When UBQLN2 was co-expressed, both cytoplasmic and nuclear hRTL8C staining co-localized extensively with UBQLN2. Compared to mRTL8A, hRTL8C showed greater overall co-localization with UBQLN2 as quantified by the Mander's overlap coefficient (MOC) (Figure S1E). Greater co-localization with UBQLN2 in the cytoplasm versus the nucleus was also observed with hRTL8C than with mRTL8A, though UBQLN2-hRTL8C puncta were observed in both compartments.

Next, we performed fluorescence recovery after photobleaching (FRAP) assays to determine whether UBQLN2-mRTL8A puncta were dynamic structures. For this, we used UBQLN2 fused to iRFP and mRTL8A fused to a small fluorescent tag, mFAP10 [41]. We identified puncta in live cells that were positive for both iRFP and mFAP10 fluorescence, photobleached the iRFP signal and measured recovery of fluorescence over time (Fig. 1F). Fluorescence recovered nearly to prebleach levels, indicating that UBQLN2-mRTL8A puncta are indeed mobile assemblies.

### RTL8 is required for efficient nuclear translocation of UBQLN2 after a heat shock

We first determined the subcellular localization of endogenous RTL8 via biochemical fractionation in HEK293 cells. We probed whole cell lysate (W), detergent-soluble cytoplasmic (C) and nuclear fractions (N), and total detergent-insoluble fraction (I) by immunoblot with a commercially available RTL8 antibody (Fig. 2A). RTL8 proteins were mainly found in the cytoplasmic fraction, however a small amount was detected in the nuclear and detergent-insoluble fractions as well. UBQLN2 was present only in the detergent-soluble fractions and mostly in the cytoplasmic fraction.

UBQLN2 is known to translocate to the nucleus under proteotoxic stress [13, 15], as well as in response to heat shock, via an unknown mechanism [19]. Given that RTL8 promotes nuclear localization of UBQLN2, we hypothesized that it may be important for stress-induced nuclear translocation of UBQLN2. To test this, we generated HEK293 cells knocked out for all RTL8 proteins using CRISPR-Cas9 (RTL8 KO). We then subjected control cells (treated with non-targeting sgRNA) and RTL8 KO cells to heat shock and performed biochemical fractionation as earlier (Fig. 2B). After heat shock, RTL8 redistributed to the nuclear and insoluble fractions from the cytoplasmic fraction, compared to cells maintained at 37 °C. The UBQLN2 signal also increased in the nuclear and insoluble fractions after heat shock, consistent with the literature [19]. By contrast, in RTL8

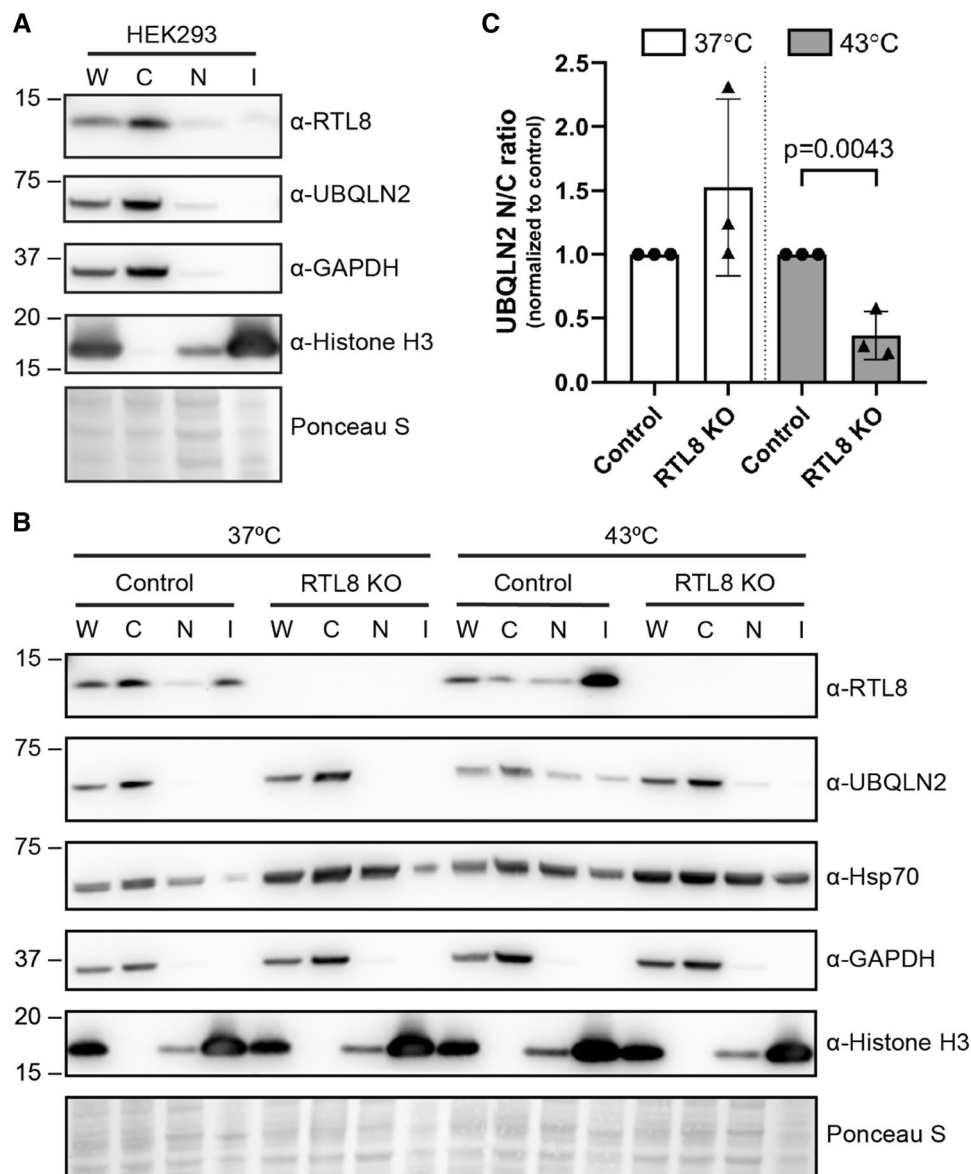


**Fig. 2** RTL8 facilitates nuclear localization of UBQLN2 following heat shock. **A** Representative immunoblot to assess subcellular distribution of endogenous RTL8 and UBQLN2 in HEK2993 cells. *W* whole cell lysate, *C* cytoplasmic detergent-soluble fraction, *N* nuclear detergent-soluble fraction, and *I* total detergent-insoluble fraction. RTL8 and UBQLN2 were predominantly in the cytoplasmic fraction. GAPDH and Histone H3 served as cytoplasmic and nuclear markers, respectively. Ponceau S staining was used to normalize loading. *N*=3 biological replicates. **B** Representative immunoblot showing RTL8-facilitated nuclear translocation of UBQLN2 following heat shock.

HEK2993 cells (control or knocked out for all RTL8 genes (RTL8 KO)) were maintained at 37 °C or heat shocked at 43 °C for 2 h. Biochemical fractionation was done as in **A**. Distribution of Hsp70 signal was used to assess efficacy of the heat shock. **C** Quantification of UBQLN2 nuclear-cytoplasmic (N/C) ratio in control and RTL8 KO cells in **B**, showing reduction of UBQLN2 nuclear translocation after heat shock in RTL8 KO cells. N/C ratio under each condition (37 °C or 43 °C) was normalized to control. Unpaired two-tailed Student's *t*-tests were used to determine statistical significance. Data are shown as mean ± SD. *N* = 3 biological replicates

KO cells we observed a marked decrease in the redistribution of UBQLN2 to the nucleus and insoluble fraction. To quantify this reduction, we calculated the nuclear-cytoplasmic (N/C) ratio of UBQLN2 under physiological (37 °C) and heat shock conditions (Fig. 2C). Cells maintained at 37 °C did not have a significant difference in the N/C ratio, whereas after heat shock we noted a significant

reduction in the N/C ratio in RTL8 KO cells compared to control cells. These data suggest that RTL8 proteins aid nuclear translocation of UBQLN2 under heat shock.

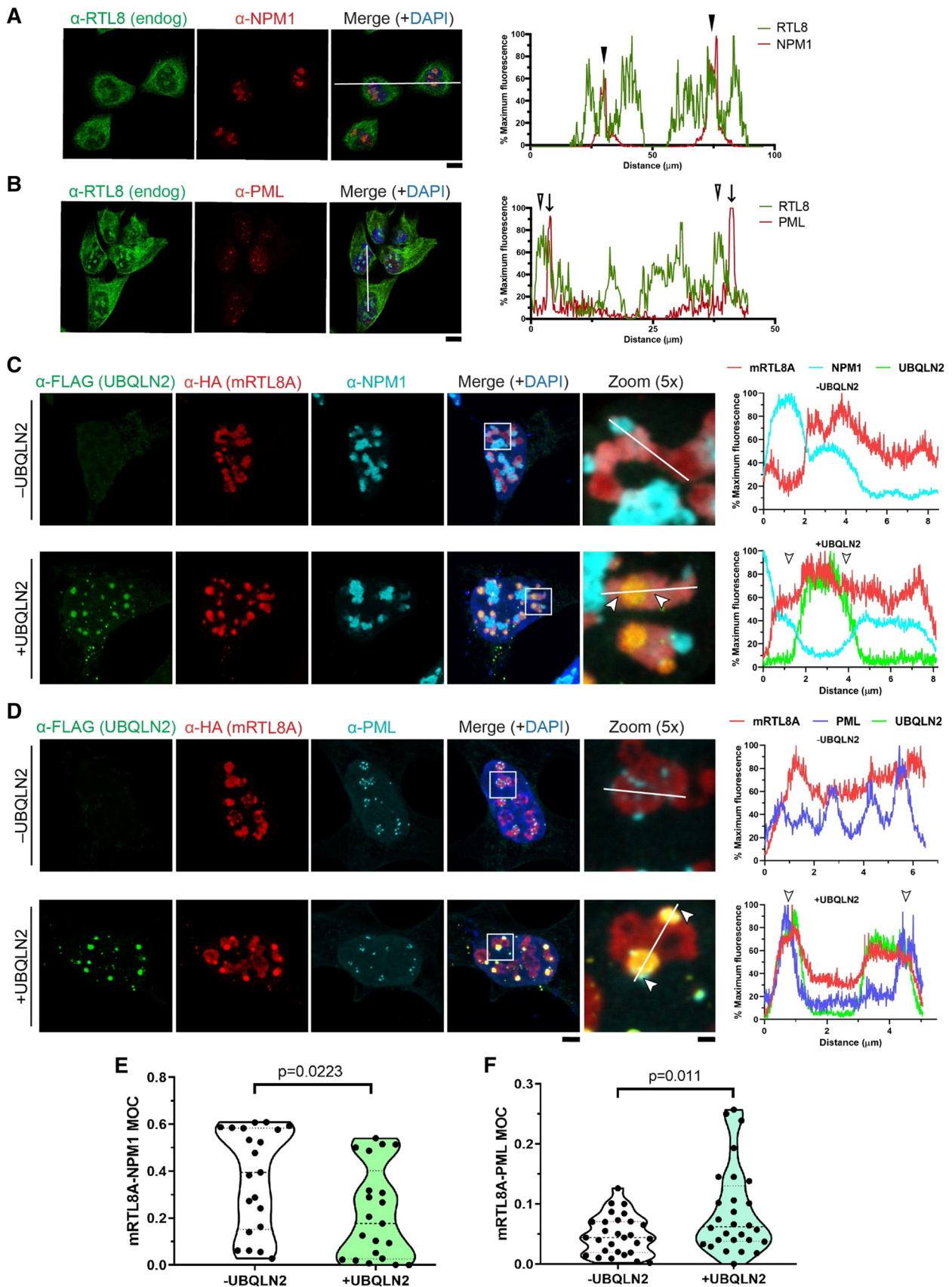


**Fig. 3** RTL8 proteins localize to nucleoli, but UBQLN2-mRTL8A subnuclear puncta are distinct from nucleoli and colocalize with PML bodies. **A** and **B** Representative immunofluorescence images assessing co-localization of endogenous RTL8 (green) with nucleoli (**A**; NPM1) and PML bodies (**B**; PML) (red), merged with DAPI (blue) (scale bars = 10  $\mu$ m). Pixel intensity plots measured across the white lines in merged images reveal coincident peak fluorescence between RTL8 and NPM1 (indicated by closed arrow heads, **A**) but not PML (arrows indicate PML peaks, open arrow heads indicate RTL8 peaks, **B**). **C** and **D** Representative images of HEK293 cells co-transfected with HA-mRTL8A (red) and either an empty vector (-UBQLN2) or one encoding FLAG-UBQLN2 (+UBQLN2) (green). Cells were stained for **C** NPM1 or **D** all PML isoforms (cyan) (scale bar for merged images = 5  $\mu$ m and zoomed images = 1  $\mu$ m). (Right) Pixel intensity plots measured across the white lines in the merged  $\times 5$  magnification images in **C** and **D**. Raw values were normalized to the maximum fluorescence value for each channel and plotted as a function of distance. White arrows in **C** represent regions surrounding UBQLN2-mRTL8A puncta that co-stain for NPM1 and mRTL8A but exclude UBQLN2. White arrows in **D** represent regions surrounding UBQLN2-mRTL8A puncta that are in close proximity with multiple PML bodies. Additional cells for NPM1 and PML staining are shown in Figure S2B and S2D, respectively. **E** and **F** Quantification of co-localization of mRTL8A with **E** NPM1 or **F** PML in the presence and absence of overexpressed UBQLN2 assessed via Mander's overlap coefficient (MOC). A reduction in NPM1 co-localization and increase in PML co-localization was observed in the presence of UBQLN2. Outliers as determined by a Grubbs' test were excluded following which unpaired two-tailed Student's *t*-tests were used to test for statistical significance. *N* = 21 and 28 cells for **E** and **F**, respectively, from two biological replicates

### UBQLN2 redistributes mRTL8A within sites of nuclear PQC

Overexpressed HA-mRTL8A concentrates in nuclear puncta (Fig. 1D, middle panel) suggesting that it partitions into specific subnuclear organelles. The co-localization with UBQLN2, a known participant in protein degradation pathways, led us to investigate whether endogenous RTL8 resides in nucleoli or PML nuclear bodies, both of which have been implicated in nuclear PQC [29–32]. Unfortunately, commercial  $\alpha$ -RTL8 antibodies do not stain endogenous RTL8 in HEK293 cells by immunofluorescence, thus we generated an  $\alpha$ -RTL8A polyclonal rabbit antibody. This antibody detected endogenous nuclear RTL8 staining in subnuclear structures that morphologically resemble those seen when HA-tagged mRTL8A is overexpressed (Fig. 1D and E). Probing with antibodies for nucleoli (Fig. 3A) or PML nuclear bodies (Fig. 3B) revealed robust localization of RTL8 to nucleoli exclusively.

Next, we sought to determine whether, as seen with endogenous RTL8, UBQLN2-mRTL8A puncta represent nucleoli. To do so, we transiently expressed mRTL8A in HEK293 cells with or without FLAG-UBQLN2. We noted intriguing changes in the subnuclear localization of mRTL8A when UBQLN2 was co-expressed. Expressed alone, mRTL8A tended to associate with the nucleolar

protein NPM1, mirroring endogenous RTL8 staining (Fig. 3C (-UBQLN2) and S2B). The heterogeneous NPM1 staining is likely due to different levels of NPM1 within distinct phase-separated compartments of nucleoli [42]. RTL8 may have a higher affinity for components within the compartment showing a weaker NPM1 signal. In contrast to endogenous RTL8, however, overexpressed mRTL8A concentrates in close proximity to PML bodies (Figs. 3D (-UBQLN2) and S2C). UBQLN2 on its own, however, did not colocalize with either NPM1 or PML (Fig. S2A). Rather, in cells expressing both UBQLN2 and mRTL8A, we see two populations of mRTL8A structures: rounded puncta that colocalize with UBQLN2 (UBQLN2-mRTL8A puncta), and larger irregular structures that do not.

The irregularly-shaped mRTL8A structures that exclude UBQLN2 are proximal to and frequently co-stain with NPM1, whereas UBQLN2-mRTL8A puncta are not positive for NPM1 (Figs. 3C (+UBQLN2), S2B and S2C). Quantification of the MOC revealed decreased co-localization of mRTL8A with NPM1 when UBQLN2 was co-expressed (Fig. 3E), suggesting that UBQLN2 sequesters mRTL8A away from nucleoli and into UBQLN2-mRTL8A puncta.

PML bodies were also observed in close proximity to UBQLN2-mRTL8A puncta, with multiple PML bodies preferentially colocalizing with and clustering around these puncta (Figs. 3D (+UBQLN2), S2D and S2E). MOC quantification displayed increased co-localization of mRTL8A with PML bodies when UBQLN2 was co-expressed (Fig. 3F). Taken together, these data indicate that UBQLN2 promotes redistribution of mRTL8A away from nucleoli and into close proximity to PML bodies.

### mRTL8A co-localizes with nuclear PQC components, both in the presence and absence of UBQLN2

The above results show that mRTL8A structures associate with nucleoli and PML bodies, both of which have been implicated in PQC. To investigate the properties of mRTL8A puncta we carried out immunostaining in transfected cells for the endogenous PQC markers Hsp70, p62/SQSTM1 (referred to as p62) and polyubiquitin, as well as for the disease-associated RNA-binding protein TDP-43. Hsp70 proteins are cytoplasmic chaperones that translocate to nucleoli during proteotoxic stress and aid in protein refolding [43, 44]. p62/SQSTM1 is an autophagy receptor that facilitates nuclear PQC by translocating to the nucleus and engaging polyubiquitinated substrates [45], and is recruited to nuclear aggregates in various neurodegenerative diseases [45, 46]. TDP-43 is known to shuttle between the nucleus and cytoplasm, accumulate in the cytoplasm in several neurodegenerative diseases [47], and form nuclear aggregates with certain proteotoxic stressors [48].



Assessed by immunofluorescence, mRTL8A co-localized extensively with Hsp70 both in the presence and absence of UBQLN2 (Figs. 4A and S3B). Hsp70 co-localization was greatest in intensely stained UBQLN2-mRTL8A puncta but was also seen in the irregular mRTL8A structures. Interestingly, infrequently observed UBQLN2-mRTL8A

cytoplasmic puncta (unfilled arrows in zoomed images in Fig. 4A and S3B) do not co-stain with Hsp70. MOC quantification revealed a small but significant decrease in mRTL8A co-localization in the presence of UBQLN2, which may be due to the lack of Hsp70 co-localization in the cytoplasm (Fig. 4B). While Hsp70 staining was seen in

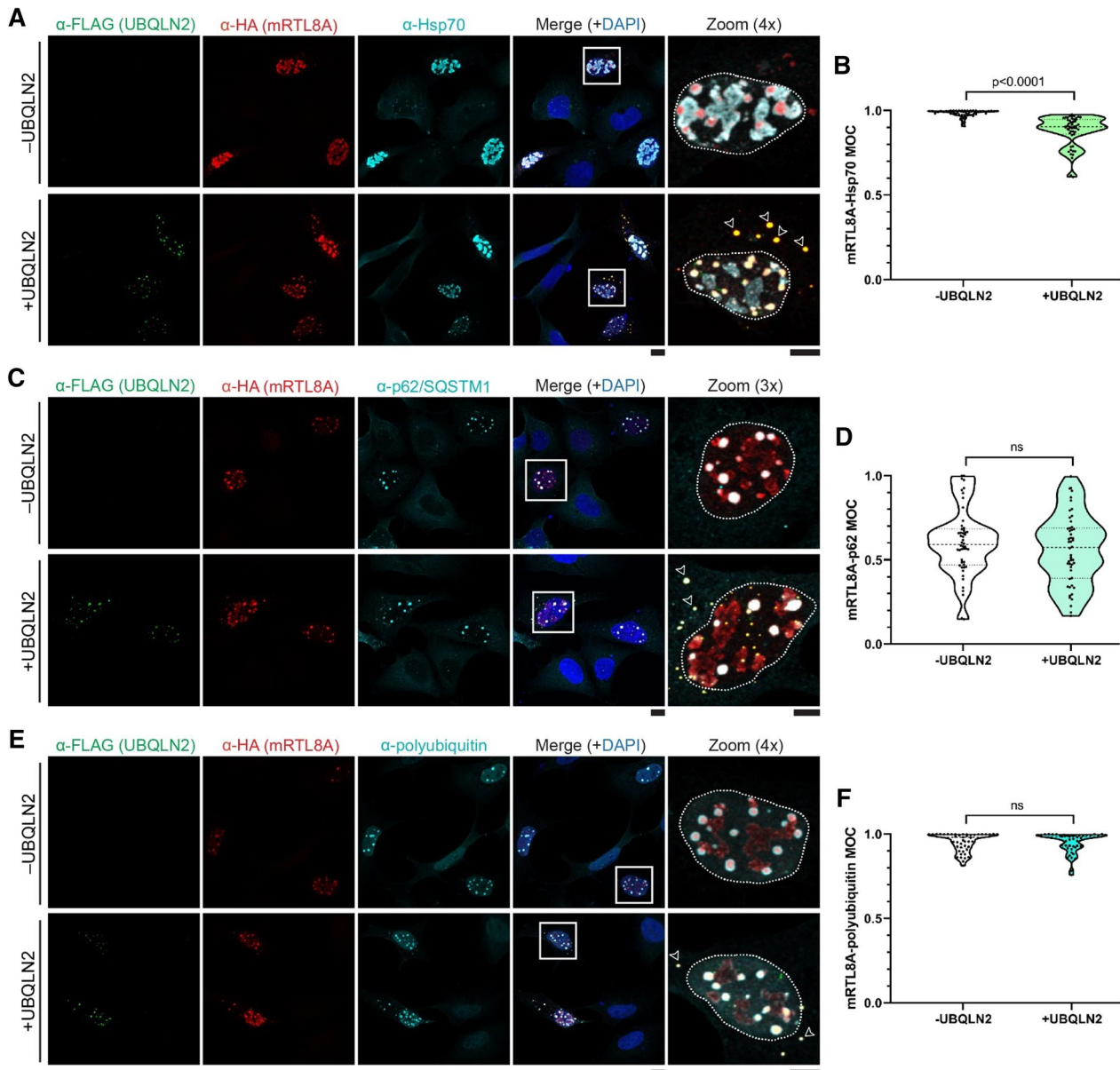


**Fig. 4** UBQLN2-mRTL8A subnuclear puncta co-localize with protein quality control markers. **A**, **C** and **E** Representative images of HEK293 cells co-transfected with HA-mRTL8A (red) and either empty vector (-UBQLN2) or FLAG-UBQLN2 (+UBQLN2) (green), and stained for **A** Hsp70, **C** p62, or **E** polyubiquitin (cyan). UBQLN2-mRTL8A nuclear puncta colocalize with all three markers. Arrowheads indicate infrequent cytoplasmic UBQLN2-mRTL8A puncta that are positive for p62 and polyubiquitin, but not Hsp70. White outlines in zoomed images represent the nucleus as determined by DAPI staining (blue in merged images). Figure S2B shows Hsp70

staining of cells expressing lower levels of FLAG-UBQLN2 and HA-mRTL8A compared to Fig. 2A (scale bar for merged images = 10  $\mu$ m and zoomed images = 5  $\mu$ m). **B**, **D** and **F** MOC quantification of co-localization of mRTL8A with **B** Hsp70, **D** p62 or **F** polyubiquitin using MOC in the presence and absence of overexpressed UBQLN2. There is significant reduction in Hsp70 co-localization in the presence of UBQLN2. Outliers as determined by a Grubbs' test were excluded. Unpaired two-tailed Student's *t* tests were used to test for statistical significance. *N* = 51, 50 and 46 cells for **B**, **D** and **F**, respectively, from two biological replicates



both types of mRTL8A structures, p62 co-localized only to the higher intensity mRTL8A puncta (Fig. 4C). There was no change in the amount of mRTL8A that co-localized with p62 in the presence of UBQLN2 (Fig. 4D). The distribution of polyubiquitin staining was similar to both Hsp70 and p62 staining (Fig. 4E). Rounded mRTL8A puncta in the absence of UBQLN2 co-stained with polyubiquitin, however irregularly-shaped mRTL8A structures did not. However, when UBQLN2 was overexpressed, both UBQLN2-mRTL8A puncta and irregular mRTL8A structures co-stained for polyubiquitin. Like with p62, no significant differences in the co-localization of polyubiquitin staining with mRTL8A were observed in the presence of UBQLN2 (Fig. 4F). UBQLN2 on its own (i.e., without overexpressed mRTL8A) colocalized only with p62 and polyubiquitin (Fig. S3A, S3C and S3D). In contrast to the above PQC markers, neither UBQLN2 nor mRTL8A colocalized with TDP-43 (Fig. S3E).

In summary, overexpressed mRTL8A concentrates in two discrete subnuclear structures containing different combinations of PQC markers. The first appear to be irregularly-shaped mRTL8A structures that co-stain for Hsp70, occasionally polyubiquitin and associate with nucleoli. The second are rounded puncta that are intensely mRTL8A-positive and co-localize with Hsp70, p62 and polyubiquitin. When co-expressed, UBQLN2 is recruited to the latter mRTL8A-positive puncta as described in Fig. 3.

### UBQLN2's interaction with mRTL8A is independent of its PXX, UBA and UBL domains but sequestration into mRTL8A puncta requires the UBA domain

To begin defining the structural requirements for UBQLN2's interaction with RTL8 we deleted two key domains of UBQLN: the UBL and UBA domains (Fig. 5A). The N-terminal UBL domain facilitates interaction with the 26S proteasome while the C-terminal UBA domain allows binding to polyubiquitinated substrates [1, 3, 8, 49, 50]. In pull-down experiments with recombinant UBQLN2 lacking either the UBA ( $\Delta$ UBA) or the UBL ( $\Delta$ UBL) (Fig. 5B), similar levels of mRTL8A were pulled down by both deletion constructs comparable to WT UBQLN2. Thus, neither the UBA nor the UBL domain is essential for UBQLN2 interaction with RTL8.

Next, we tested whether deleting the UBL, UBA, or the PXX domain affected the ability of UBQLN2 to co-localize with mRTL8A and translocate to the nucleus. The proline-rich PXX repeat region of unknown function is unique to UBQLN2 among brain-expressed UBQLNs and is particularly linked to neurodegenerative disease [51]. To understand whether co-localization with mRTL8A requires UBQLN2's ability to bind polyubiquitinated substrates, we also included the ubiquitin-binding deficient UBQLN2-L619A mutant [19,

25], which is unable to bind ubiquitin in pulldown experiments (Fig S4A).

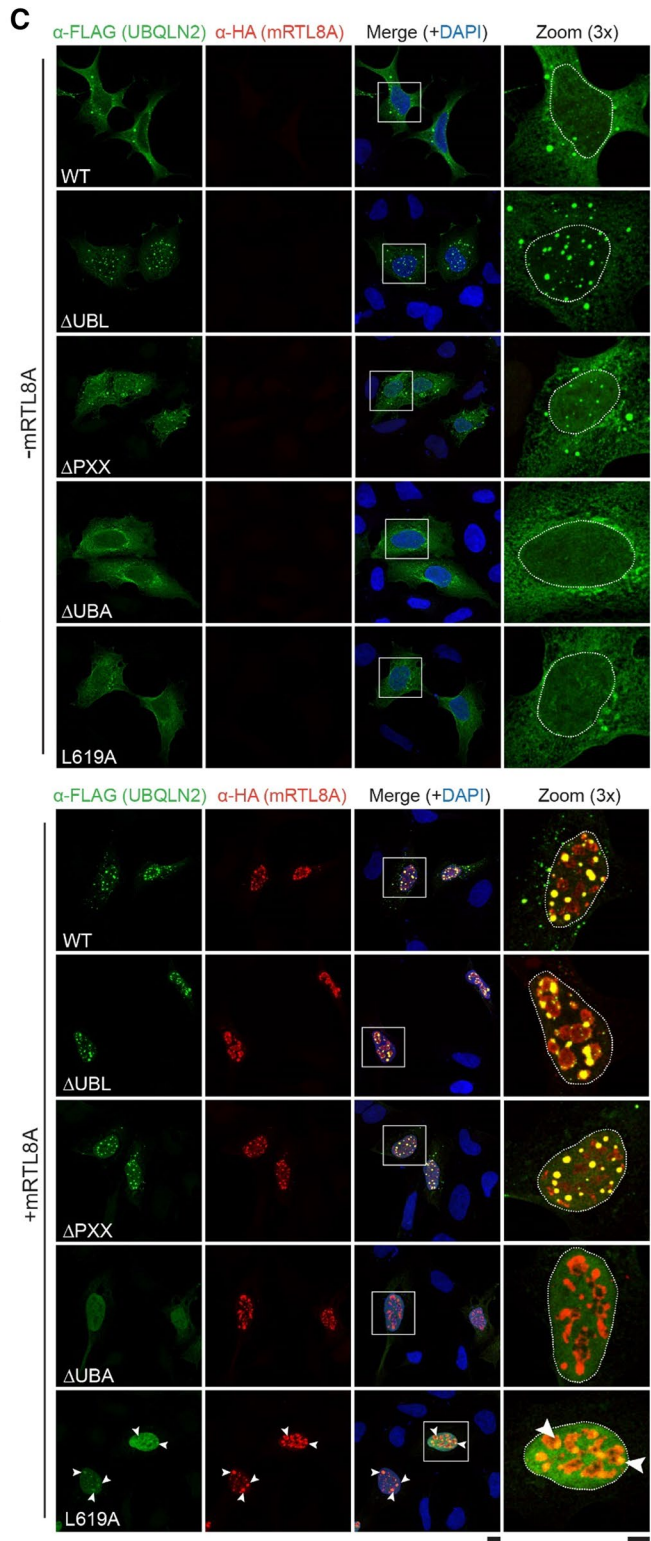
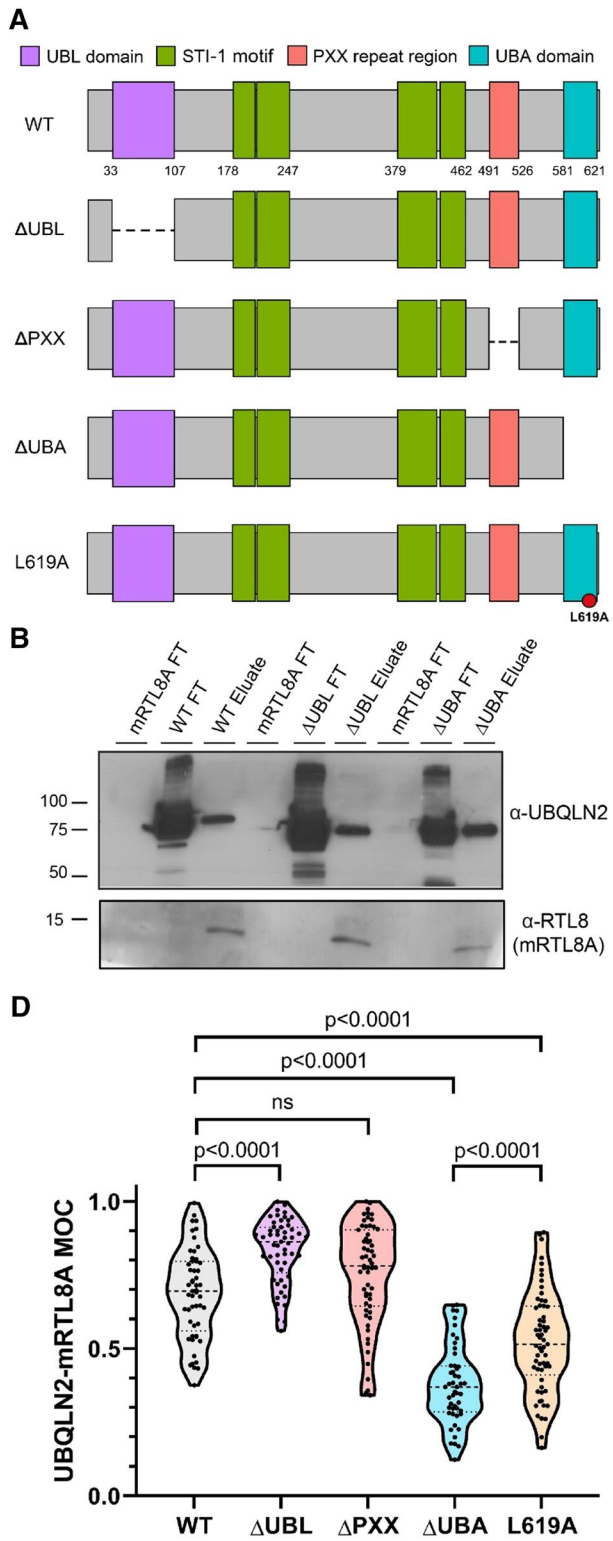
In the absence of co-expressed mRTL8A, cells expressing WT UBQLN2,  $\Delta$ UBA,  $\Delta$ PXX and L619A showed a similar distribution, predominantly in the cytoplasm with faint diffuse staining to, in some cases, speckle-like staining in the nucleus (Fig. 5C, top).  $\Delta$ UBA UBQLN2, however, did not form cytoplasmic puncta, consistent with our previous observations [19, 25].  $\Delta$ UBL UBQLN2 was present in both the cytoplasm and nucleus where it formed larger and more intense puncta.

When co-expressed with mRTL8A,  $\Delta$ UBL and  $\Delta$ PXX UBQLN2 behaved like WT UBQLN2 in translocating to the nucleus (Fig. 5C, bottom).  $\Delta$ UBL UBQLN2 also showed a statistically significant increase in co-localization with mRTL8A compared to WT UBQLN2 (Fig. 5D). In contrast,  $\Delta$ UBA UBQLN2 did not colocalize with mRTL8A even though its nuclear localization was promoted by mRTL8A. Instead,  $\Delta$ UBA UBQLN2 distributed diffusely in the nucleus and was excluded from nuclear mRTL8A puncta (also see Figures S4B and S4C). MOC quantification supported our observations, revealing a statistically significant decrease in case of  $\Delta$ UBA UBQLN2 versus WT UBQLN2. L619A UBQLN2 showed an intermediate phenotype between WT and  $\Delta$ UBA UBQLN2. Like WT UBQLN2, L619A UBQLN2 translocated into the nucleus and co-localized with mRTL8A puncta (also see Figures S4D and S4E), but a significant proportion of L619A remained diffuse in the nucleus, resembling  $\Delta$ UBA UBQLN2 distribution. Quantification confirmed these observations, with mRTL8A having significantly higher MOC with L619A UBQLN2 than with  $\Delta$ UBA UBQLN2, but significantly lower than seen with WT UBQLN2.

Taken together, these results imply that neither the UBA nor UBL domain is required for UBQLN2 to directly bind mRTL8A, but the UBA domain is required for UBQLN2's incorporation into mRTL8A subnuclear puncta. Furthermore, polyubiquitin binding does not appear to be essential for UBQLN2 recruitment into mRTL8A puncta.

### Preferential interactions of RTL8 with UBQLN2 reveal functional heterogeneity among UBQLNs

Other UBQLN family members, including UBQLN1 and UBQLN4, share conserved structural domains with UBQLN2 except for the proline-rich repeat region (PXX) (Figure S5A). This similarity prompted us to test whether mRTL8A also co-localizes with or aids UBQLN1 and UBQLN4 translocation to the nucleus. When expressed alone in HEK293 cells, UBQLN1 and UBQLN4 exhibited subcellular distributions distinct from UBQLN2 (Fig. 6A, upper panels). Whereas UBQLN2 was present mostly in cytoplasmic puncta with rare speckle-like nuclear staining,



both UBQLN1 and UBQLN4 showed both diffuse cytoplasmic and nuclear staining. When individual UBQLNs were overexpressed with mRtL8A, UBQLN2 typically co-localized with mRtL8A, primarily in the nucleus, whereas

UBQLN1 showed highly variable co-localization (Fig. 6A, lower panels) and UBQLN4 did not co-localize appreciably with mRtL8A. Using MOC to quantify co-localization, we confirmed significant differences in mRtL8A

**Fig. 5** UBQLN2's UBA domain is dispensable for interaction with mRTL8A, but required for UBQLN2 incorporation into mRTL8A subnuclear puncta. **A** Schematic depicting wild-type (WT) UBQLN2, various domain deletion constructs lacking the UBL domain ( $\Delta$ UBL), PXX repeat region ( $\Delta$ PXX) or UBA domain ( $\Delta$ UBA), and the ubiquitin binding-deficient L619A mutation (represented as a red circle). **B** Pull-down of recombinant His-mRTL8A by recombinant full-length GST-UBQLN2 full-length WT,  $\Delta$ UBL, and  $\Delta$ UBA proteins. The flow-through (FT) and eluate were visualized on an immunoblot with  $\alpha$ -UBQLN2 (*top*) or  $\alpha$ -RTL8 antibodies (*bottom*). **C** Representative images of transfected HEK293 cells expressing HA-mRTL8A (red) and either FLAG-UBQLN2 WT,  $\Delta$ UBL,  $\Delta$ PXX,  $\Delta$ UBL or L619A (green). White outlines in zoomed images delimit the nucleus as determined by DAPI staining (blue in merged images). White arrows in cells expressing FLAG-UBQLN2 L619A and HA-mRTL8A indicate partial co-localization of UBQLN2 and mRTL8A in the nucleus (scale bar for merged images = 10  $\mu$ m and zoomed images = 5  $\mu$ m). **D** Quantification of co-localization of WT or domain-deleted UBQLN2 constructs with mRTL8A. MOC was calculated for each cell expressing both constructs in a field of view. Outliers as determined by a Grubbs' test were excluded, following which a one-way ANOVA ( $p < 0.0001$ ) and a Tukey's multiple comparisons test were performed to identify statistically significant differences among MOCs.  $N = 53, 53, 59, 49$  and  $61$  cells for WT,  $\Delta$ UBL,  $\Delta$ PXX,  $\Delta$ UBA and L619A UBQLN2, respectively, from two biological replicates

co-localization with UBQLNs 1, 2 and 4 (Fig. 6B). We also quantified the nuclear to cytoplasmic (N/C) ratio of all three UBQLNs (Fig. 6C). In the absence of exogenous mRTL8A, UBQLN2 had the lowest N/C ratio, with the two other UBQLNs having N/C ratios closer to one. Co-expression of mRTL8A led to an almost two-fold increase in the N/C ratio of UBQLN2 with no appreciable effect on the N/C ratio of UBQLN1 or UBQLN4.

Next, we tested whether this significant difference in co-localization reflects differences in the ability of the various UBQLNs to bind mRTL8A. To rule out the influence of endogenously expressed UBQLN proteins, we used HEK293 cells with all three UBQLNs knocked out (UBQLN TKO). When co-expressed with mRTL8A, UBQLN2 most robustly immunoprecipitated mRTL8A, followed by UBQLN4 and UBQLN1 (Fig. 6D and E). These results, together with our immunofluorescence results, support preferential interaction of RTL8s with UBQLN2 over other brain expressed UBQLNs.

A recent study demonstrated that UBQLN TKO cells have no detectable RTL8 protein levels [36]. We confirmed this loss of RTL8 protein expression in TKO cells (Figure S5B). Using these cells, we assessed whether expressing UBQLN1, UBQLN2 or UBQLN4 separately could restore endogenous RTL8 protein levels. Based on the above results, we hypothesized that UBQLN2 would rescue RTL8 levels to the greatest extent. Indeed, UBQLN2 was most efficient in rescuing RTL8 levels while UBQLN1 partially rescued RTL8 levels and UBQLN4 had no effect (Fig. 6F and G).

This rescue was not the result of increased RTL8 gene expression (Figure S5D), implying that UBQLN2 stabilizes RTL8 proteins.

To determine if this differential effect held true in a more physiologically relevant model, we examined RTL8 levels in brain lysates from UBQLN1, UBQLN2 and UBQLN4 knockout mice. While in UBQLN2 knockout mice RTL8 protein was undetectable, both UBQLN1 and UBQLN4 knockout mice showed RTL8 levels similar to that of WT non-transgenic (nonTg) mice (Fig. 6H). Thus, in mouse brain neither UBQLN1 nor UBQLN4 can compensate for the loss of UBQLN2. Conversely, endogenous UBQLN2 expression is sufficient to maintain RTL8 levels in UBQLN1 or UBQLN4 knockout mice. These data suggest that the functional interaction between RTL8 and UBQLN2 does not extend to other brain expressed UBQLNs.

## Discussion

UBQLN2 is known to participate in cytoplasmic PQC through the UPS and autophagy. It is less clear what role UBQLN2 plays in the nucleus, to which it translocates under various stress conditions [12, 13, 15, 19]. Nuclear aggregates of disease proteins, including known UBQLN2 substrates, are common in various neurodegenerative diseases. Previous work in yeast has demonstrated that the UBQLN2 ortholog, Dsk2, is specifically required for clearance of misfolded nuclear proteins [52]. Conceivably, the recruitment of UBQLN2 to the nucleus facilitates the degradation of misfolded proteins associated with some neurodegenerative proteinopathies.

Among ubiquilins, UBQLN4 reportedly functions in DNA double-stranded break repair [53], but a common nuclear function across the ubiquilin family is unknown. Here, we identified a novel UBQLN2-interacting protein, RTL8, that regulates UBQLN2's translocation to and behavior in the nucleus and underscores functional heterogeneity within the UBQLN protein family.

RTL8 is a small protein of unknown function expressed in the cytoplasm and nucleus. Endogenous nuclear RTL8 localizes to nucleoli, which are condensates associated with ribosome maturation [54–56] and protein quality control [29, 55, 57]. When overexpressed, mRTL8A tends to concentrate in the nucleus and frequently co-localizes to nucleoli as well as to ubiquitin-enriched subnuclear structures distinct from nucleoli. Overexpressed mRTL8A also recruits and sequesters UBQLN2 in highly dynamic puncta that appear to represent phase-separated condensates. In the nucleus, UBQLN2-mRTL8A condensates contain other PQC proteins including p62. Recently, p62-containing nuclear condensates were shown to be sites of proteasome-mediated



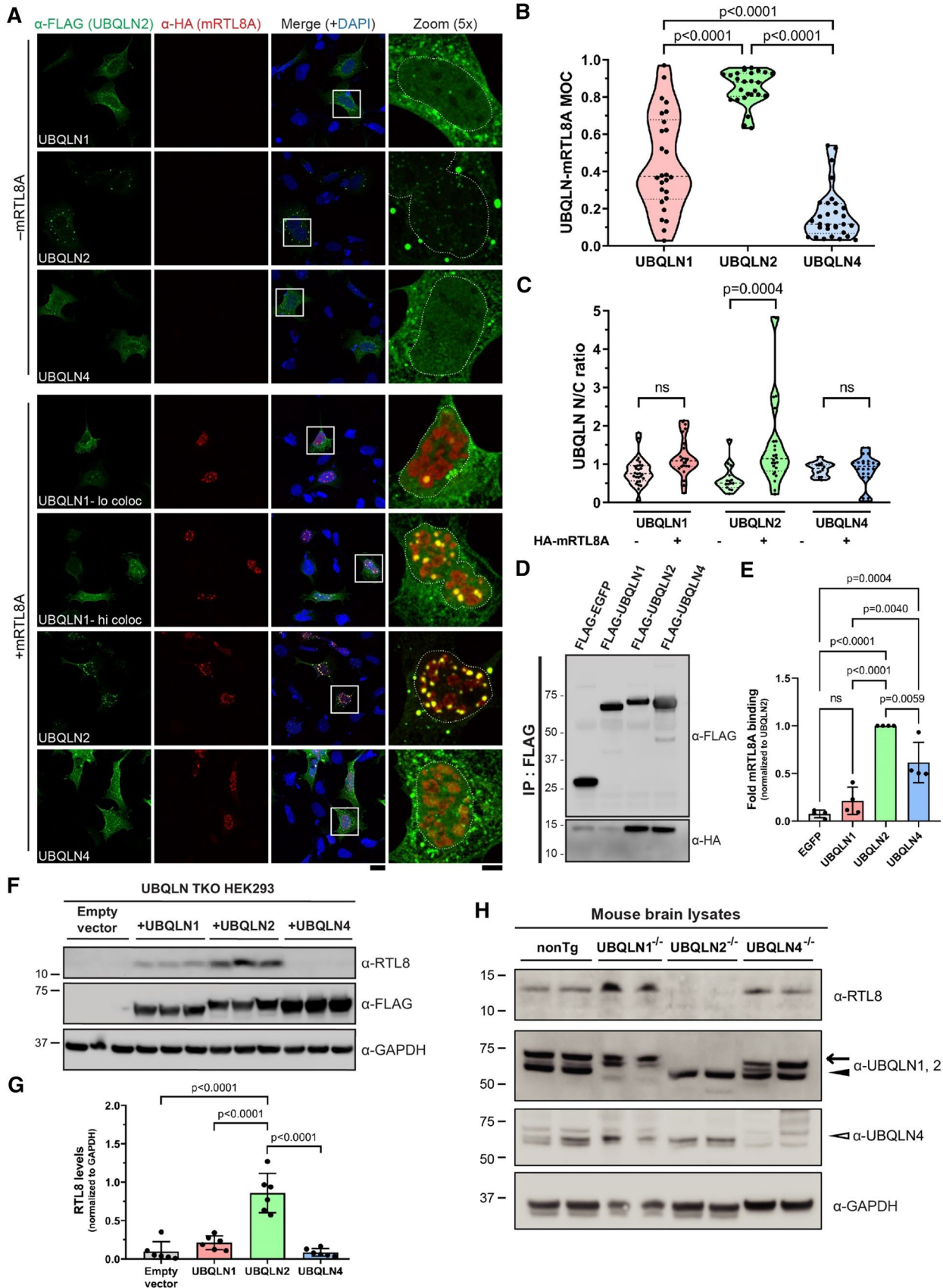


**Fig. 6** Among brain-expressed ubiquilins, UBQLN2 preferentially interacts with mRTL8A and regulates endogenous RTL8 levels in cells and mouse brain tissue. **A** Representative immunofluorescence images of HEK293 cells co-transfected with HA-mRTL8A (red) and either FLAG-tagged UBQLN1, UBQLN2 or UBQLN4 (green), shown merged with DAPI (blue). White outlines in the zoomed images delimit the nucleus, determined by DAPI staining. Representative images of high and low co-localization of UBQLN1 with mRTL8A are included to illustrate the wide range of observed co-localization for UBQLN1 (*lo coloc* low co-localization, *hi coloc* high co-localization) (scale bar for merged images = 20  $\mu$ m and zoomed images = 5  $\mu$ m). **B** Quantification of co-localization of UBQLN1, UBQLN2 or UBQLN4 with mRTL8A. MOC was calculated for each cell expressing both constructs in a field of view. UBQLN2 had significantly higher MOC compared to the other UBQLNs. Outliers as determined by a Grubbs' test were excluded, following which a one-way ANOVA ( $p < 0.0001$ ) and a Tukey's multiple comparisons test were performed to identify statistically significant differences among Mander's correlation coefficients.  $N = 26, 27$  and  $31$  cells for UBQLN1, UBQLN2 and UBQLN4, respectively, from two biological replicates. **C** Quantification of UBQLN nuclear localization, represented by the ratio of nuclear to cytoplasmic (N/C) fluorescence intensity. UBQLN2 had a significantly higher N/C ratio in the presence of mRTL8A. Statistical significance was determined by first excluding outliers as determined by a Grubbs' test and then performing a one-way ANOVA ( $p < 0.0001$ ) followed by a Tukey's multiple comparisons test.  $N = 28, 15$  and  $14$  cells for UBQLN1, UBQLN2 and UBQLN4, respectively, without mRTL8A and  $25, 24$  and  $24$  cells for UBQLN1, UBQLN2 and UBQLN4, respectively, with mRTL8A. 2 biological replicates were used in both cases. **D** Representative immunoblot showing co-immunoprecipitation of mRTL8A by UBQLNs. HEK293 cells knocked out for UBQLN1, UBQLN2 and UBQLN4 (UBQLN TKO) were transfected to express HA-mRTL8A and either FLAG-tagged UBQLN1, UBQLN2, UBQLN4 or EGFP as a control. Co-immunoprecipitation was assessed by anti-FLAG pull down. Lysate input levels are shown in Figure S5C. **E** Quantification of mRTL8A co-immunoprecipitated by the various UBQLNs as shown in **D**. UBQLN2 showed greater mRTL8A pull-down than other UBQLNs. The amount of mRTL8A pulled down was normalized to the FLAG signal in the eluates. Data are shown as mean  $\pm$  SD, normalized to UBQLN2.  $N = 4$  biological replicates. **F** Representative immunoblots for endogenous RTL8 levels in TKO cells transfected either with an empty vector, FLAG-tagged UBQLN1, UBQLN2 or UBQLN4. GAPDH was used as a loading control. **G** Quantification of the rescue of RTL8 levels shown in (**F**), normalized to GAPDH levels. UBQLN2 showed greater rescue of RTL8 than other UBQLNs. Statistical significance as determined by a one-way ANOVA ( $p < 0.0001$ ) followed by a Tukey's multiple comparisons test. Data are shown as mean  $\pm$  SD, normalized to UBQLN2.  $N = 6$  per condition. **H** Immunoblot of brain lysates from non-transgenic (nonTg), UBQLN1<sup>-/-</sup>, UBQLN2<sup>-/-</sup> and UBQLN4<sup>-/-</sup> mice. In case of UBQLN1 and 2, arrowhead denotes the band for UBQLN1 while the arrow points to the band for UBQLN2. GAPDH was used as a loading control

protein degradation [58], supporting our hypothesis that UBQLN2-RTL8 condensates participate in nuclear UPS. Among brain-expressed ubiquilins, only UBQLN2 shows mRTL8A-dependent nuclear recruitment and co-localization: by contrast, mRTL8A colocalizes with UBQLN4 and UBQLN1 only rarely or occasionally, respectively, and fails to promote nuclear translocation of either. Furthermore,

UBQLN2 stabilizes levels of RTL8 protein in mouse brain, which is not the case for UBQLN1 and UBQLN4. Of the three brain expressed UBQLNs, only the loss of UBQLN2 reduces RTL8 levels, supporting a physiological role for the interaction between these two proteins. The variable degree of co-localization of UBQLN1 with mRTL8A raises the possibility that hetero-dimerization of UBQLN1 with UBQLN2 could promote an indirect interaction between mRTL8A and UBQLN1. If that were the case, however, we would expect no UBQLN1-mRTL8A interaction in cells lacking UBQLN2. Instead, in TKO cells individually transfected with UBQLN proteins, both UBQLN4 and UBQLN1 can interact with mRTL8A, albeit at significantly lower levels than UBQLN2. We suggest that while mRTL8A preferentially regulates UBQLN2 translocation to the nucleus over UBQLN1 or UBQLN4, protein domains common to the three UBQLNs do contribute to UBQLN-mRTL8A binding.

The small number of replicates in our MS screen identifying RTL8 as a potential interactor and the need to employ overexpression in our analysis of RTL8 because of the lack of specific antibodies suitable for detecting endogenous RTL8 are limitations to the current study. We were nonetheless able to validate the direct interaction between mRTL8A and UBQLN2 through recombinant protein pull-downs and immunoprecipitation from mouse brain lysate. Given the approximately sevenfold enrichment of RTL8 in our study, it is notable that earlier MS screens for UBQLN2 interactors did not identify RTL8 [7, 19]. One possible explanation for this discrepancy is that our MS screen was performed in HEK293 cells which contain multiple copies of the q arm of the X chromosome, the locus of the RTL8 gene family. Thus, HEK293 cells likely express higher levels of RTL8 than other cell models or tissues, enabling detection in our screen. Recent literature also supports our findings: a proteomics study examining the effects of mutations or knockout of UBQLN2 identified RTL8 as one of two gag/pol proteins highly regulated by UBQLN2 [36].

Multiple structural motifs in UBQLN2 could mediate the direct interaction with RTL8 including the ubiquitin-like domain (UBL), the ubiquitin-associated domain (UBA), the four ST11 motifs, and the proline-rich repeat (PXX) region. Our recombinant protein pull-down and immunofluorescence experiments establish that mRTL8A functionally interacts with UBQLN2 independent of the UBA or UBL domains and does not depend on ubiquitin binding. These findings suggest regions outside of these domains regulate the interaction of RTL8 and UBQLN2. The preferential interaction of mRTL8A with UBQLN2 over UBQLN1 and UBQLN4, initially pointed to the distinctive PXX region of UBQLN2 as a potentially critical structural feature. However, a deletion construct of UBQLN2 lacking the PXX region colocalized with mRTL8A to the same degree as WT

UBQLN2, establishing that the UBQLN2-mRTL8A interaction does not require the PXX region.

Additional data support the conclusion that UBQLN2-mRTL8A binding and mRTL8A-mediated functional modulation of UBQLN2 are not regulated by a single unique domain in UBQLN2. First, overexpressed UBQLN1 partially colocalizes with mRTL8A and rescues endogenous RTL8 levels in UBQLN knockout cells, albeit much less so than UBQLN2. While this data contrasts with our finding that UBQLN1 does not stabilize RTL8 levels in mouse brain, we suspect that overexpressed UBQLN1 engages in a lower-affinity interaction with RTL8 via domains that are shared with UBQLN2. This hypothesis is supported by the finding that both UBQLN1 and UBQLN4 immunoprecipitate with mRTL8A when UBQLN2 is not present. Second, although mRTL8A directly interacts with recombinant  $\Delta$ UBA UBQLN2 and recruits overexpressed  $\Delta$ UBA UBQLN2 into the nucleus,  $\Delta$ UBA UBQLN2 does not co-localize with mRTL8A nuclear puncta. We conclude that the UBA domain is not required for direct UBQLN2-mRTL8A binding but is necessary for functional modulation of UBQLN2 behavior – namely, recruitment into nuclear puncta associated with PQC proteins. We and others have shown that the UBA domain of UBQLN2 is critical for UBQLN2 LLPS [25, 59] and hypothesize that while  $\Delta$ UBA UBQLN2 can bind mRTL8A, it is excluded from nuclear condensates formed by mRTL8A due to its inability to phase separate. The ubiquitin-binding UBQLN2 mutant, L619A, has been shown to decrease UBQLN2 LLPS [59] while  $\Delta$ UBL UBQLN2 shows enhanced LLPS [25, 59]. The data is consistent with our finding that L619A UBQLN2 shows decreased co-localization with mRTL8A puncta compared to WT, while  $\Delta$ UBL UBQLN2 has increased co-localization with mRTL8A puncta (Fig. 5). The degree of co-localization of UBQLN2 with RTL8 condensates could impact UBQLN2 participation in UPS activity within nuclear condensates. Thus, our data support a model in which binding to RTL8 and functional modulation of UBQLN2 by RTL8 are mediated by nonidentical regions within UBQLN2.

Identifying the specific motifs that mediate RTL8 interaction with and functional modulation of UBQLN2 will offer insight into how RTL8 regulates UBQLN2 function in health and dysfunction in disease. For example, only UBQLN2 contains the PXX repeat region in which the majority of fALS-causing UBQLN2 mutations are found. While our data show the PXX repeat region is not required for mRTL8A binding, some mutations within the PXX repeat region alter UBQLN2 LLPS [25, 60] and could interfere with its recruitment into nuclear RTL8 puncta, with potential implications for disease. Although ubiquitin binding to the UBA domain appears not to be required for RTL8 binding and nuclear recruitment of UBQLN2, RTL8 binding to

UBQLN2 could modulate ubiquitin binding. Intriguingly, all three UBQLNs undergo phase separation and are inherently aggregate-prone [61], and the UBA domain itself may seed UBQLN oligomerization and aggregation [25]. A systematic study of structural motifs and disease mutations in UBQLN2 will be required to determine which regions are critical for binding and whether fALS mutations impact RTL8 binding and RTL8-dependent properties of UBQLN2.

Our results support a role for RTL8 in facilitating UBQLN2 nuclear translocation under stress. Knocking out RTL8 significantly decreases the amount of UBQLN2 in the nucleus after heat shock. Both endogenous RTL8 and overexpressed mRTL8A localize to the nucleolus, a membraneless organelle recently implicated in nuclear UPS [29], and when co-expressed, mRTL8A and UBQLN2 colocalize in nuclear puncta that recruit PQC markers. Both findings are consistent with the hypothesis that RTL8 contributes to nuclear PQC pathways. RTL8 may also have functional roles beyond PQC. In addition to being implicated in the UPS, nucleoli are also sites of ribosome maturation [54–56], so RTL8 might be involved in ribosome biogenesis. Consistent with both possibilities, RTL8 could recruit UBQLN2 to nucleoli to facilitate the turnover of proteins involved in ribosome biogenesis.

Endogenous human RTL8 resides in both the nucleus and cytoplasm, but under heat shock the proportion of RTL8 in the nucleus is significantly increased. When overexpressed, however, mRTL8A localizes almost entirely to the nucleus. This discrepancy in subcellular localization between human endogenous RTL8 and mouse RTL8A could be due to one of several factors: (1) mRTL8A possesses a canonical NLS in its N-terminal domain that human RTL8 lacks; (2) artificially high levels of transiently overexpressed mRTL8A could influence its localization; (3) our transfected mRTL8A construct lacks the 3' UTR which may be important for proper subcellular localization of certain proteins, as with the immediate-early gene Activity-regulated cytoskeletal associated protein (Arc) [62].

RTL8 associate with nucleoli and are in close proximity to and/or colocalize with PML bodies when overexpressed. PML bodies perform diverse functions in the nucleus, including serving as sites of proteasomal degradation [30, 63, 64]. As opposed to nucleoli, which are constitutive PQC compartments [29], PML bodies are thought to serve as stress inducible PQC compartments [30]. Substrate proteins targeted to PML bodies tend to be SUMOylated, with the PML protein itself acting as a SUMO E3 ligase [64]. There is extensive interconnectivity between SUMOylation and ubiquitination pathways [65–67], highlighting a potential role for UBQLN2 in shuttling substrates that may be SUMOylated and/or ubiquitinated. Since mRTL8A resides in close proximity to PML bodies, it may facilitate



recruitment of UBQLN2 to this nuclear site of proteasomal degradation. Alternatively, the PML clustering we observe could represent a byproduct of protein aggregation rather than a specific functional role for mRTL8A [63, 68]. RTL8 proteins, including mRTL8A, have a predicted SUMOylation site (Lys85) which may target them for degradation (<http://jassa.fr/>) [69]. We do not think that PML clustering is an artifact of mRTL8A aggregation, however, based on unpublished control studies which assessed PML clustering on mutant TDP-43 which forms nuclear aggregates [70] and is itself a target for SUMOylation [71, 72]. This data suggests that the PML clustering on mRTL8A puncta is more complex than PML-mediated degradation of aggregated proteins. Further experiments will be required to clarify the significance of this observed PML clustering.

UBQLN2 has been implicated in a wide range of neurodegenerative diseases, with nuclear aggregates of misfolded proteins representing a signature pathological feature for several of them [12, 13, 15, 19]. Understanding the role that UBQLN2 plays in nuclear PQC and the mechanisms and critical components that regulate it will require further study. The data presented here show that RTL8, a novel protein that binds UBQLN2, drives UBQLN2 into the nucleus where they together form condensates that recruit PQC components. RTL8 is important for the nuclear translocation of UBQLN2 under heat shock. The interaction of RTL8 with UBQLN2 and its regulation of UBQLN2 behavior is selective for this particular UBQLN2 over UBQLN1 and UBQLN4. Future investigation into the significance of the UBQLN2-RTL8 interaction and whether it is affected by known human disease mutations may help decipher the mechanisms by which UBQLN2 dysfunction leads to neurodegenerative disease.

## Materials and methods

### Mass spectrometry (MS) and data analysis

UBQLN2 complexes were isolated from HEK293 cells overexpressing FLAG-tagged wild-type UBQLN2 using anti-FLAG M2 Affinity Gel (Millipore-Sigma, A2220). After washing, the gel beads were eluted with FLAG peptide and the eluates were analyzed at the University of Michigan Mass Spectrometry-Based Proteomics Resource Facility (<https://www.pathology.med.umich.edu/proteomics-resource-facility>).

Upon cysteine reduction (10 mM dithiothreitol (DTT)) and alkylation (65 mM 2-chloroacetamide or iodoacetamide, with similar results) of the cysteines, the isolated proteins

were digested overnight with sequencing grade modified trypsin (Promega). The resulting peptides were resolved on a nano-capillary reverse phase column (PicoFrit column, New Objective) using a 1% acetic acid/acetonitrile gradient at 300 nL/min and directly introduced into a linear ion-trap mass spectrometer (LTQ Orbitrap XL, Thermo Fisher). Data-dependent MS/MS spectra on the five most intense ions from each full MS scan were collected (relative collision energy ~ 35%).

Proteins and peptides were identified by searching the data against *H. sapiens* protein database containing only the canonical, reviewed protein entries (Swiss-Prot, 20,286 entries; downloads release 2020\_05) using Proteome Discoverer (v2.4, ThermoFisher Scientific). Enzyme specificity was set to fully tryptic digestion with up to two missed cleavages. Search parameters included a precursor and fragment mass tolerances of 50 ppm and 0.6 Da, respectively. Carbamidomethylation of cysteine was considered fixed modification. Oxidation of methionine, deamidation of asparagine and glutamine, and ubiquitination (diglycine remnant) on lysine residues were considered as variable modifications. Percolator, a peptide-to-spectrum (PSM) validator, was used to filter the protein/peptides to retain only those with a false discovery rate (FDR) of  $\leq 1\%$ .

To correct for missing/zero PSM values in control samples since natural log of zero leads to a numerical error, an empirical value of 1 was added to PSM values of both control and FLAG-UBQLN2 datasets. Data analysis was done on RStudio (v 1.2.5033) using the normalized spectrum abundance factor (NSAF) method outlined by Zybailov and colleagues [73]. Each protein's PSM value was first normalized to its length, denoted as length normalized PSM. Next, the length-normalized PSM value for each protein was divided by the sum of all length normalized PSMs for the given sample, denoted as NSAF. To calculate fold enrichment over control, NSAF values for each hit from a FLAG-UBQLN2 dataset were normalized to their respective control PSM values. These values were then  $\log_2$  transformed and tested for significance using a Student's *t* test. Volcano plot was generated using the ggplot2 package [74] by plotting  $\log_2$  transformed fold enrichment values and negative  $\log_{10}$  transformed *p* values on the *x* and *y* axes, respectively. The *p* value threshold was expanded to 0.15 ( $-\log_{10}$  value of 0.8239) to prevent the exclusion of possible interactors since only two replicates were used for this analysis. Hits with a  $\log_2$  transformed fold enrichment of greater than 1.5 and a *p* value of 0.15 ( $-\log_{10}$  value of 0.8239) were considered possible interactors and are shown in red.

## Antibodies

The antibodies used in the study and their dilutions are indicated in the table below.

Antibody	Source	Dilution (IB—immunoblotting, IF—immunofluorescence)
<b>Primary antibodies</b>		
Rabbit polyclonal $\alpha$ -FAM127B/RTL8A (detects all RTL8 proteins)	Proteintech #20282-1-AP	1:500 (IB)
Custom made rabbit polyclonal $\alpha$ -FAM127B/RTL8A (detects all RTL8 proteins)	GenScript (immunogen sequence: MEGQGKVKRP-KAYMC)	1:250 (IB), 1:100 (IF)
Rabbit polyclonal $\alpha$ -FLAG	Millipore Sigma #F7425	1:1000 (IF)
Mouse monoclonal $\alpha$ -FLAG	Millipore Sigma #F1804	1:2000 (IB)
Rat monoclonal $\alpha$ -FLAG Alexa Fluor™ 488/555-conjugated	Thermo Fisher # MA1142-A488/MA1142-AF555	1:200 (IF)
Mouse monoclonal $\alpha$ -GAPDH	Millipore Sigma #MAB374	1:5000 (IB)
Rabbit polyclonal $\alpha$ -HA	Santa Cruz #sc-805	1:500 (IF)
Mouse monoclonal $\alpha$ -HA	BioLegend #901513	1:1000 (IF)
Rabbit polyclonal $\alpha$ -histone H3	Cell Signaling #4499S	1:5000 (IB)
Mouse monoclonal $\alpha$ -Hsp70	Abcam # ab5439	1:2000 (IB), 1:1000 (IF)
Mouse monoclonal $\alpha$ -NPM1	Thermo Fisher #32-5200	1:1000 (IF)
Guinea pig polyclonal $\alpha$ -p62/SQSTM1	Progen #GP62-C	1:500 (IF)
Mouse monoclonal $\alpha$ -PML Alexa Fluor™ 647-conjugated (detects all PML isoforms)	Santa Cruz #sc-377390 AF647	1:50 (IF)
Rabbit polyclonal $\alpha$ -TDP-43	Proteintech #10782-2-AP	1:200 (IF)
Rabbit polyclonal $\alpha$ -UBQLN1/2	Novus Biologicals #NBP1-56536	1:1000 (IB)
Mouse monoclonal $\alpha$ -UBQLN2	Novus Biologicals #NBP2-25164	1:2000 (IB), 1:1000 (IF)
Mouse monoclonal $\alpha$ -A1Up (UBQLN4)	Santa Cruz #sc-136145	1:2000 (IB)
Mouse monoclonal $\alpha$ -polyubiquitylated proteins (FK1)	Millipore #04-262	1:500 (IF)
Rabbit polyclonal $\alpha$ -ubiquitin	Cell Signaling #3933S	1:1000 (IB)

Antibody	Source	Dilution (IB—immunoblotting, IF—immunofluorescence)
<b>Secondary antibodies</b>		
Goat $\alpha$ -mouse IgG(H+L) HRP-conjugated	Jackson ImmunoResearch #115-035-146	1:2000 (IB)
Goat $\alpha$ -rabbit IgG(H+L) HRP-conjugated	Jackson ImmunoResearch #111-035-144	1:2000 (IB)
Goat $\alpha$ -mouse IgG(H+L) Alexa Fluor™ 488/594/647-conjugated	Thermo Fisher #A11001/A11004/A21235	1:1000 (IF)
Goat $\alpha$ -rabbit IgG(H+L) Alexa Fluor™ 488/594/647-conjugated	Thermo Fisher #A11008/A11037/A21244	1:1000 (IF)
Goat $\alpha$ -guinea pig IgG(H+L) Alexa Fluor™ 647-conjugated	Thermo Fisher #A21450	1:1000 (IF)
Goat $\alpha$ -mouse IgM Alexa Fluor™ 647-conjugated	Thermo Fisher #A21238	1:1000 (IF)

## Plasmids

The pCMV4-FLAG-UBQLN2 plasmid (p4455 FLAG-hPLIC-2; Addgene plasmid #8661) and pCS2-FLAG-UBQLN1 plasmid (p4458 FLAG-hPLIC-1; Addgene plasmid #8663) were gifts from Dr. Peter Howley [75]. UBQLN4 was cloned from pDONR223-UBQLN4 (pENTR-A1UP; Addgene plasmid #16170), which was a gift from Dr. Huda Zoghbi (Baylor College of Medicine; [76]), into the pCMV4-FLAG vector. FLAG-UBQLN2  $\Delta$ UBL and  $\Delta$ PXX were custom-made from VectorBuilder Inc. and were constructed on a pRP(Exp) backbone with a CMV promoter. The  $\Delta$ UBL plasmid lacked the UBL domain (residues 33–107) and the  $\Delta$ PXX plasmid lacked the PXX repeat region (residues 491–526). FLAG-UBQLN2  $\Delta$ UBA was made by mutating arginine 581 to a stop codon in the pCMV4-FLAG-UBQLN2 vector using QuickChange II site-directed mutagenesis (Agilent) with primers 5'-GCTGCCGAATCCAGAAGTCTAATTTTCAGCAACAACGGAA-3' and 5'-TTCCAGTTGTTGCTGAA ATTAGACTTCTGGATTTCGGCAGC-3'. UBQLN2 L619A mutation was introduced into pCMV4-FLAG-UBQLN2 using site directed mutagenesis as described previously [25]. Mouse RTL8A cDNA was PCR amplified from first stand cDNA synthesized from RNA isolated from wild-type C57BL/6 mouse brain using primers 5'-ATGGAAGGCCAAGGCAAGGTA

AAG-3' and 5'-CTAGAAGTCCTCATCCTCCTCCCACCC GAAC-3' and cloned into the pCMV-HA vector downstream of the HA tag using restriction sites EcoRI and KpnI. For recombinant protein studies, UBQLN2 and mRTL8A were subcloned into the pET-28 vector backbone downstream of the His-tag using restriction sites BamHI and HindIII. GST-tagged UBQLN2 full length and deletion constructs were subcloned from iRFP-UBQLN2 constructs described previously [25] into the pGEX4T vector downstream of the GST tag. mFAP10-mRTL8A and HA-hRTL8C were custom-made from VectorBuilder Inc. and were constructed on a pRP(Exp) backbone with a CMV promoter. A HA-tag along with mFAP10 (sequence obtained from Addgene #159463) was inserted before the N-terminus of mRTL8A (CCDS30134.1) followed by a 3xGS linker. For hRTL8C (NM\_001078171.2), a HA-tag was inserted on the N-terminus before the first residue.

### Recombinant protein expression, purification and pulldown

UBQLN2 and mRTL8A constructs were transformed in Rosetta (DE3) *Escherichia coli*. All Luria–Bertani (LB)/agar plates and LB media were supplemented with 50 µg/ml kanamycin and 34 µg/ml chloramphenicol. Transformed cells were grown overnight at 37 °C on LB/agar plates. On the following day, cells were transferred to 100 ml LB starter cultures and allowed to grow for 60–90 min. The starter cultures were then transferred to 2 l flasks containing 1 l LB media. After the OD reached  $A_{600} \approx 0.6$ –0.8, cells were induced with 0.5 mM isopropyl  $\beta$ -D-1-thiogalactopyranoside (IPTG) and collected after 3–5 additional hours of incubation. The bacteria were collected by centrifugation for 6 min at  $10,322 \times g$ . Bacterial pellets were stored at  $-80$  °C until purification.

**For WT and L619A UBQLN2-ubiquitin pulldown:** His-UBQLN2 pellets from WT and L619A UBQLN2 expressing *E. coli* were resuspended in pre-chilled lysis buffer (25 mM sodium phosphate, 0.5 M sodium chloride, 20 mM imidazole pH 7.4, cOmplete™ Mini EDTA-free Protease Inhibitor Cocktail (Sigma Aldrich), 6 µl/ml of saturated phenylmethylsulfonyl fluoride (PMSF) in ethanol, 1 mg/ml lysozyme, and 10% glycerol). Bacteria were then lysed using EmulsiFlex B-15 high pressure homogenizer (Avestin). The lysate was centrifuged at  $31,000 \times g$  for 25 min. The proteins were precipitated from the supernatant by adding 0.2 g/mL ammonium sulfate. The solution was stirred at 4 °C for 30 min and centrifuged at  $13,000 \times g$  for 25 min. The pellets were re-dissolved in buffer containing 25 mM sodium phosphate, 0.5 M sodium chloride, 20 mM imidazole pH 7.4, filtered through 0.22 µm Steriflip vacuum filters (Millipore) and subsequently loaded on a HisTrap HP column (GE Healthcare Life Sciences) using 25 mM sodium phosphate,

0.5 M sodium chloride, 20 mM Imidazole pH 7.4 as the binding buffer. The protein was eluted by running a 0–100% gradient of 25 mM sodium phosphate, 0.5 M sodium chloride, 0.5 M Imidazole pH 7.4. Eluates were assessed on Western blot and probed for UBQLN2 and ubiquitin.

**For GST-UBQLN2 and His-mRTL8A pulldown:** GST-tagged UBQLN2 bacteria pellets (Full length,  $\Delta$ UBA and  $\Delta$ UBL) pellets were resuspended in pre-chilled lysis buffer and lysed. Lysates were applied to GST agarose column (Glutathione agarose resin, GoldBio) and washed three times in wash buffer (1× TBS + 1 mM DTT). His-tagged mRTL8A bacteria pellets were resuspended in pre-chilled lysis buffer containing and lysed as described above. The lysates from the homogenizer were added to Ni-NTA agarose (Qiagen) and incubated on the nutator at 4 °C for 1 h. Then the beads with the bound protein were washed twice with wash buffer (1× TBS, 10 mM imidazole, pH 8.0). Beads were then mixed with elution buffer (1× TBS, 250 mM imidazole, pH 8.0) and incubated on a nutator for 30 min at 4 °C. The slurry was spun at  $700 \times g$  for 3 min and the supernatant with the eluted protein was collected. Purified His-mRTL8A was applied to GST agarose column and incubated at 4 °C. Column was washed three times in wash buffer (1× TBS + 1 mM DTT) and eluted with 10 mM reduced glutathione in wash buffer. Eluates were evaluated by immunoblotting and probed for UBQLN2 and mRTL8A.

### Transgenic mice

UBQLN1<sup>-/-</sup> mice were generated through the University of Michigan Transgenic Animal Core. CRISPR/Cas9 was used to delete UBQLN1 exons 2 and 3 which introduces a premature stop codon after splicing from exon 1–4. This ablates protein expression by nonsense mediated mRNA decay. Primers for genotyping for UBQLN1: UBQLN1<sup>-/-</sup> FWD—5'-CTT GGC AAT AGG CAT TGA ATG AAA GAA GT-3', UBQLN1<sup>-/-</sup> REV—5'-CAT CTC TTA ACC AAT GAG CTG TCT CTC C-3' and UBQLN1 WT REV—5'-GTA CAG TAC CAC CCA GAC TG-3'. Wild type mice for UBQLN1 amplify a band at 350 bp. Homozygous knockout mice generate a band at 550 bp and heterozygote mice amplify two bands, one at 350 bp and another at 550 bp. UBQLN4<sup>-/-</sup> mice were a generous gift from Dr. Huda Zoghbi (Baylor College of Medicine). UBQLN4<sup>-/-</sup> mice were generated from ES cell line XG905 (RRID: CVCL\_PW18) (BayGenomics) created with a gene trap vector containing a splice-acceptor sequence upstream of the reporter gene,  $\beta$ -geo (a fusion of  $\beta$ -galactosidase and neomycin phosphotransferase II) splice. 5' RACE sequencing identified the insertion site of the gene trap vector downstream of exon 5 of the UBQLN4 gene. UBQLN4<sup>-/-</sup> mice are genotyped using primers UBQLN4  $\beta$ -geo FWD—5'-ATC TTC CTG AGG CCG ATA-3' and UBQLN4  $\beta$ -geo Rev 5'-GTC AAA



TTC AGA CGG CAA AC-3' which prime within the  $\beta$ -geo reporter gene and amplify a band of 250 bp.  $\beta$ -Geo positive mice are further determined to be either UBQLN4 KO heterozygotes or homozygotes by Western blot of brain lysate probed for the absence of the UBQLN4 protein. UBQLN2 WT-low and UBQLN2<sup>-/-</sup> mice and their genotyping were used as previously described [22, 25].

### Cell culture, CRISPR knockout and transient transfection

HEK293 (ATCC CRL-1573; Batch #70008735) were maintained in DMEM (HyClone™ DMEM/high glucose + L-glutamine, +glucose, -sodium pyruvate, Cytiva Life Sciences) supplemented with 10% fetal bovine serum (Atlanta Biologicals) and 1X Penicillin/Streptomycin (Invitrogen). HEK293 T-rex control and UBQLN1, UBQLN2, and UBQLN4 knock out (TKO) cells were kindly provided by Dr. Ramanujan Hegde (Medical Research Council (MRC) Laboratory of Molecular Biology; [20]) and maintained in DMEM supplemented with 10% fetal bovine serum, 10  $\mu$ g/ml Blastidicin S (Fisher), and 100  $\mu$ g/ml hygromycin B (Fisher). All lines were maintained and passaged in 5% CO<sub>2</sub>.

CRISPR reagents were obtained from Horizon Discovery unless otherwise mentioned. Early passage HEK293 cells were transfected with either non-targeting crRNA or crRNA targeting all RTL8 paralogs (5'-GTTCTCGTCCAC GAACATGT-3'; designed using Broad Institute's sgRNA Designer tool), tracrRNA and Cas9-EGFP mRNA using DharmaFECT Duo as per manufacturer's instructions. 24 h post transfection, cells were FACS-sorted gating on EGFP fluorescence at a 1 cell/well dilution onto a 96 well plate. Clones that grew to confluency were picked and RTL8 knock out was verified by qPCR and immunoblotting for RTL8.

All described plasmids were transfected into cells using FuGENE® HD Transfection Reagent (Promega) according to the manufacturers protocol. Briefly, media was replaced with fresh complete DMEM prior to adding FuGENE/DNA mix to cells. FuGENE and DNA mixes were separately prepared in OptiMEM Reduced Serum Medium (Gibco) while maintaining a FuGENE to DNA ratio of 3:1 and incubated for 5 min at room temperature. FuGENE/DNA master mix was prepared by adding FuGENE to DNA. This mixture was incubated for 30 min at room temperature prior to addition to cells.

### Immunoblotting

Protein samples in 1X Laemmli buffer containing 100 mM DTT were resolved by gel electrophoresis on acrylamide NuPAGE Novex 4–12% Bis-Tris protein gels (Invitrogen) with NuPAGE MES SDS running buffer (Invitrogen). Gels were subsequently transferred onto 0.2  $\mu$ m nitrocellulose

membranes at 100 V for 1 h. Membranes were immediately rinsed with deionized H<sub>2</sub>O, stained with Ponceau S and imaged on a G Box Mini imager (Syngene). Membranes were rinsed with 1X Tris-buffered saline, 0.1% (TBST) for 10 min, and blocked with 5% non-fat dry milk (DotScientific) and 0.05% BSA (Fisher) in 1X TBST for 1 h. Membranes were incubated overnight with shaking in the cold with primary antibodies diluted with 5% milk and 0.05% BSA in 1X TBST). Membranes were rinsed three times with 1X TBST for 10 min, incubated at room temperature with secondary antibodies for 1 h, and then rinsed three times with 1X TBST for 10 min prior to developing with Western Lightning® Plus ECL (Fisher) or EcoBright Nano/Femto HRP 50 (Innovative Solutions) using the G Box Mini imager set to ECL auto exposure. GeneSys (Syngene) was used for blot quantification and raw values were normalized to their respective loading controls.

### Mouse brain dissection

All animal procedures were done in accordance with the Institutional Animal Care and Use Committee (IACUC) standards at the University of Michigan. Animals were deeply anesthetized with a ketamine/xylazine mixture and perfused transcardially with 0.1 M phosphate buffer. Brains were dissected and lysates were prepared in RIPA buffer (Sigma) supplemented with PMSF, protease and phosphatase inhibitors (Sigma Aldrich). Brain tissue was homogenized, centrifuged (13,000 rpm for 30 min) and the supernatants were collected. For immunoblotting, protein concentration was measured using a BCA assay (Thermo Scientific). Samples were prepared in 1X Laemmli sample buffer before loading or storing at -20 °C for later use. For immunoprecipitation experiments, brain lysates were used the same day as they were prepared.

### Co-immunoprecipitation (co-IP)

#### In vitro co-IP

TKO cells were co-transfected with HA-mRTL8A and FLAG-tagged EGFP, UBQLN1, UBQLN2, or UBQLN4 expression plasmids. On ice, transfected TKO cells were harvested 48 h post transfection with NETN buffer (150 mM NaCl, 5 mM EDTA, pH 8.0, 50 mM Tris, pH 8.0, 1.0% NP-40 IGEPAL CA-630) supplemented with PMSF and protease inhibitors (Sigma Aldrich). Cells were lysed at 4 °C on a rotator and centrifuged at maximum speed for 15 min. An aliquot of soluble supernatants was collected for input levels prior to the complexing of remaining total soluble protein with  $\alpha$ -FLAG antibody and Protein A/G Plus-Agarose beads (Santa Cruz) overnight at 4 °C. Beads were washed with

NETN buffer and combined with 2× Laemmli buffer, boiled and processed for immunoblotting. Inputs were combined with 1× Laemmli buffer and processed similarly, representing 1/10th of the soluble protein material used for co-IPs. Quantification values represent a ratio of immunoprecipitated mRTL8A to the immunoprecipitated EGFP, UBQLN1, UBQLN2, and UBQLN4, background subtracted and normalized to EGFP.

### In vivo co-IP

Brain lysates from transgenic UBQLN2-low mice [25] were pre-cleared with Protein A agarose beads slurry (Thermo Scientific) rotating at 4 °C for 1 h. The lysate was centrifuged at 4000 rpm at 4 °C for 30 min and the supernatant (pre-cleared lysate) was removed. The pre-cleared lysate was incubated with anti-FLAG M2 affinity gel beads (250 µl) (Sigma Aldrich) rotating at 4 °C for 3 h. The beads were washed three times with PBS and centrifuged at 4000 rpm at 4 °C and the PBS was discarded. Proteins were eluted by incubating the anti-Flag beads in 2× Laemmli buffer at 100 °C for 5 min. The supernatant was collected after centrifugation at 4000 rpm and saved for immunoblot analysis.

### Heat shock and biochemical fractionation

2 million HEK293 cells were seeded 48 h prior to fractionation. For a heat shock, cells were placed in an incubator (with 5% CO<sub>2</sub>) set to 43 °C for 2 h. Cells were then washed with ice cold 1× PBS. Whole cell lysate was prepared by sonicating one-tenth volume of the total cell pellet for 10 s in 1× Laemmli buffer followed by centrifugation at maximum speed for 10 min. The supernatant was immediately boiled for 10 min. Biochemical fractionation was done using NE-PER extraction reagents (Thermo Scientific) supplemented with Halt Protease Inhibitor Cocktail (Thermo Scientific) as per the manufacturer's instructions with modifications as outlined below. After obtaining the nuclear soluble fraction, the remaining pellet was washed thrice in ice cold PBS. 1× Laemmli buffer was added to the pellet and sonicated for 10 s, following which centrifugation and boiling was carried out as before. This was termed the total insoluble fraction. 10 µg of protein from each fraction as determined by a 660 nm assay (Thermo Scientific) was used for immunoblotting. Blots were probed using indicated antibodies with GAPDH and Histone H3 serving as cytoplasmic and nuclear markers, respectively.

### Immunofluorescence

Cells were seeded onto 12 mm poly-D-lysine coated coverslips (Neuvitro Corporation) 24 h prior to transfection. FuGENE/DNA mix was replaced with fresh supplemented

DMEM 6 h post transfection. 24 h post transfection, cells were washed with 1× PBS and fixed with 4% PFA in 1× PBS. Excess PFA was neutralized using 50 mM glycine in PBS. Coverslips were then permeabilized and blocked in 10% normal goat serum (Vector Labs) in 1× PBS containing 0.1% Triton X-100 and 0.05% BSA (PBTGS) and incubated with primary antibodies diluted in PBTGS overnight at 4 °C with shaking. For primary antibodies not conjugated to fluorophores, coverslips were washed in PBS prior to incubation with secondary antibodies (diluted in PBTGS) and DAPI for 1 h at room temperature with shaking. After washing three times in PBS, coverslips were mounted on glass slides using Prolong Glass (Invitrogen), sealed with Covergrip sealant (Biotium) and allowed to cure for 24 h prior to imaging. Z-stack images were acquired on a Leica Stellaris 5 confocal microscope using an Airyscan detector and a 63× or 100× oil objective or a Nikon A1 confocal microscope using a 63× oil objective. Subsequent analyses were done on ImageJ (NIH, v1.53c).

### Quantification of co-localization, pixel intensity plot generation and measurement of nuclear-cytoplasmic ratio

To quantify co-localization, Mander's correlation coefficients on a region of interest were obtained using the Just Another Co-localization Plugin (JACoP) [77] on ImageJ with thresholding within a channel kept constant across replicates. Statistical significance was ascertained using a Student's *t* test or one-way ANOVA as applicable. For generating pixel intensity plots, maximum intensity projections of z-stacks were generated on ImageJ. An ROI was specified using the line tool across each channel and the plot profile feature was used. The raw values obtained from each channel were normalized to the maximum value of the particular channel and plotted as a function of distance in µm. Quantification of nuclear UBQLN1, 2 and 4 was performed using Cell Profiler, an open-source cell imaging analysis software (<https://cellprofiler.org/>) [78]. Nuclear fluorescence intensity of UBQLN proteins was quantified by measuring the degree of co-localization of FLAG-tagged UBQLN with the DAPI signal. Cytoplasmic fluorescence intensity was measured by determining ROI based on UBQLN staining excluding the nucleus. The ratio of the nuclear to cytoplasmic fluorescence intensity was plotted across different UBQLNs in the presence and absence of overexpressed mRTL8.

### Fluorescence recovery after photobleaching

HEK293 cells were plated on LAB-TEK II borosilicate chambers slides and transfected with iRFP-UBQLN2, mFAP10-mRTL8A and mApple. 24 h after transfection, the transfection media was changed to media containing 40 µM

of DFHBI-1T (Sigma Aldrich) and incubated for 30 min at 37 °C. Cells were washed 2× with warm media and then imaged with a Nikon A-1 confocal microscope using Nikon Elements software with perfect focus engaged. FRAP imaging consisted of three phases: pre-bleach imaging, bleaching, and post-bleach imaging. During pre-bleach imaging, an iRFP-UBQLN2/mFAP10-mRTL8A punctum was imaged twice at and 8.3 s interval. In the bleach phase, an ROI was drawn corresponding to 1/3 to 1/2 the area of a punctum. This ROI defined the stimulation area for a 647 nm laser at 30% power. The postbleach phase consisted of two periods. For the first minute, images were acquired every 8.3 s, while for the subsequent 10 min images were acquired every 10 s. Images were analyzed in ImageJ by drawing an ROI surrounding the bleached region and the entire punctum. Average fluorescence intensity was measured for both ROI and recovery of the bleached area was plotted as a percentage of the average punctum intensity to account for iRFP photobleaching during the course of imaging.

### Assessment of RTL8 levels in UBQLN knockout HEK293 cells

HEK293 UBQLN1,2,4, total knock out (TKO) cells were plated on 6-well plates, transfected with indicated plasmids and harvested 48 h post transfection. Cells were washed with 1× PBS and lysed for 5 min in cold 1× RIPA buffer (Thermo Scientific) supplemented with PMSF and protease inhibitors (Sigma Aldrich) Samples were sonicated and centrifuged at 22,000×g for 30 min at 4 °C. Soluble supernatant fractions were collected and protein concentration was determined by the Pierce BCA assay (Thermo Scientific). 20 µg of protein from all samples were used for immunoblotting.

### Quantitative PCR

Cells were washed with ice cold RNase-free PBS prior to RNA extraction. Total RNA from cells was isolated using an RNEasy kit (Qiagen) and on column genomic DNA digestion was done as per manufacturer's instructions. 1 µg total RNA was then used for first strand cDNA synthesis (Applied Biosystems) using manufacturer supplied random primers. cDNA was used at a 1:10 dilution, along with gene specific primers and SYBR Green Master Mix (Applied Biosystems) for qPCR. qPCR reactions and SYBR green detection were carried out on QuantStudio 3 (Applied Biosystems) using the comparative  $\Delta\Delta C_t$  mode. Additional data analysis was done on Microsoft Excel and Prism. *GAPDH* and *ACTB* were used as housekeeping controls in all reactions. Primers used are as follows: pan *RTL8* (detects all *RTL8* paralogs): Forward—5'-TCCCGGAGTTCATCGTGC-3', Reverse—5'-CTAGAAGTCCTCGTCTCCTCCC-3'; *GAPDH*: Forward—5'-CTGACTTCAACAGCGACACC-3',

Reverse—5'-TAGCCAAATTCGTTGTCATAC C-3' and *ACTB*: Forward—5'-CACCATTGGCAATGAGCGGTTCC-3', Reverse—5'-AGGTCTTTGCGGATGTCCACGT-3'.

### Alignment and sequence comparison

Human and mouse RTL8 sequences were obtained from UniProt (Accession IDs—Q9BWD3 (hRTL8A), Q17RB0 (hRTL8B), A6ZKI3 (hRTL8C), Q9D1F0 (mRTL8A/B) and Q9D6I0 (mRTL8C)). Alignment was conducted with the ESPript 3.0 web tool (<http://esprict.ibcp.fr>) [79]. Percentage identity matrix based on sequence identity was generated using Clustal Omega. (<https://www.ebi.ac.uk/Tools/msa/clustalo>).

### Statistical analysis

All statistical tests were carried out on GraphPad Prism 8 software (Graphpad Software Inc.). The significance threshold was set at  $p=0.05$ , unless indicated otherwise. Details regarding specific statistical analysis are included in the figure legends.

**Supplementary Information** The online version contains supplementary material available at <https://doi.org/10.1007/s00018-022-04170-z>.

**Acknowledgements** We thank Peter Howley and Huda Zoghbi for providing constructs, Huda Zoghbi for providing the UBQLN4 *-/-* mouse line and Ramanujan Hegde for providing the ubiquilin triple knockout cell line. We also thank Magdalena Ivanova and Sami Barmada for their helpful suggestions and critical feedback.

**Author contributions** Conceptualization: HM, AP, HP, LS. Methodology: HM, AP, HT, CZ, XZ, NS, VB, LS. Investigation: HM, AP, HT, CZ, XZ, EC, RP, NS, LS, BT. Writing: HM, HP, LS. Funding Acquisition: LS, HP. Resources: LS, YZ, HP. Supervision: HP, YZ, LS.

**Funding** This work was supported by NIH 9R01NS096785-06, 1P30AG053760-01, The Amyotrophic Lateral Sclerosis Foundation and the UM Protein Folding Disease Initiative.

**Availability of data and material** The authors confirm that the data supporting the findings in this are available within the article, at repository links provided within the article, and within its supplementary files. The authors agree to share reagents, cell lines and animal models used in this study upon request.

**Code availability** Not applicable.

### Declarations

**Conflict of interest** None declared.

**Ethics approval** All animal experiments were conducted under the approval of The University of Michigan Institutional Animal Care & Use Committee, protocol number PRO00010103.



**Consent to participate** Not applicable.

**Consent for publication** Not applicable.

## References

- Saeki Y, Saitoh A, Toh-e A, Yokosawa H (2002) Ubiquitin-like proteins and Rpn10 play cooperative roles in ubiquitin-dependent proteolysis. *Biochem Biophys Res Commun* 293(3):986–992. [https://doi.org/10.1016/S0006-291X\(02\)00340-6](https://doi.org/10.1016/S0006-291X(02)00340-6)
- Massey LK, Mah AL, Ford DL, Miller J, Liang J, Doong H et al (2004) Overexpression of ubiquilin decreases ubiquitination and degradation of presenilin proteins. *J Alzheimers Dis* 6:79–92. <https://doi.org/10.3233/JAD-2004-6109>
- Seok Ko H, Uehara T, Tsuruma K, Nomura Y (2004) Ubiquilin interacts with ubiquitylated proteins and proteasome through its ubiquitin-associated and ubiquitin-like domains. *FEBS Lett* 566(1–3):110–114. <https://doi.org/10.1016/j.febslet.2004.04.031>
- Kaye FJ, Modi S, Ivanovska I, Koonin EV, Thress K, Kubo A et al (2000) A family of ubiquitin-like proteins binds the ATPase domain of Hsp70-like Stch. *FEBS Lett* 467(2–3):348–355. [https://doi.org/10.1016/S0014-5793\(00\)01135-2](https://doi.org/10.1016/S0014-5793(00)01135-2)
- N'Diaye EN, Kajihara KK, Hsieh I, Morisaki H, Debnath J, Brown EJ (2009) PLIC proteins or ubiquilins regulate autophagy-dependent cell survival during nutrient starvation. *EMBO Rep* 10(2):173–179. <https://doi.org/10.1038/embor.2008.238>
- Rothenberg C, Srinivasan D, Mah L, Kaushik S, Peterhoff CM, Ugolino J et al (2010) Ubiquilin functions in autophagy and is degraded by chaperone-mediated autophagy. *Hum Mol Genet* 19(16):3219–3232. <https://doi.org/10.1093/hmg/ddq231>
- Alexander EJ, Ghanbari Niaki A, Zhang T, Sarkar J, Liu Y, Nirujogi RS et al (2018) Ubiquilin 2 modulates ALS/FTD-linked FUS-RNA complex dynamics and stress granule formation. *Proc Natl Acad Sci USA* 115(49):E11485–E11494. <https://doi.org/10.1073/pnas.1811997115>
- Zhang D, Raasi S, Fushman D (2008) Affinity makes the difference: nonselective interaction of the UBA domain of ubiquilin-1 with monomeric ubiquitin and polyubiquitin chains. *J Mol Biol* 377(1):162–180. <https://doi.org/10.1016/j.jmb.2007.12.029>
- Dao TP, Kolaitis RM, Kim HJ, O'Donovan K, Martyniak B, Colicino E et al (2018) Ubiquitin modulates liquid-liquid phase separation of UBQLN2 via disruption of multivalent interactions. *Mol Cell* 69(6):965e6–978. <https://doi.org/10.1016/j.molcel.2018.02.004>
- Dao TP, Castaneda CA (2020) Ubiquitin-modulated phase separation of shuttle proteins: does condensate formation promote protein degradation? *BioEssays*. <https://doi.org/10.1002/bies.202000036>
- Brettschneider J, Van Deerlin VM, Robinson JL, Kwong L, Lee EB, Ali YO et al (2012) Pattern of ubiquilin pathology in ALS and FTLN2 indicates presence of C9ORF72 hexanucleotide expansion. *Acta Neuropathol* 123(6):825–839. <https://doi.org/10.1007/s00401-012-0970-z>
- Mori F, Tanji K, Odagiri S, Toyoshima Y, Yoshida M, Ikeda T et al (2012) Ubiquilin immunoreactivity in cytoplasmic and nuclear inclusions in synucleinopathies, polyglutamine diseases and intranuclear inclusion body disease. *Acta Neuropathol* 124(1):149–151. <https://doi.org/10.1007/s00401-012-0999-z>
- Zeng L, Wang B, Merillat SA, Minakawa EN, Perkins MD, Ramani B et al (2015) Differential recruitment of UBQLN2 to nuclear inclusions in the polyglutamine diseases HD and SCA3. *Neurobiol Dis* 82:281–288. <https://doi.org/10.1016/j.nbd.2015.06.017>
- Yang H, Yue H-W, He W-T, Hong J-Y, Jiang L-L, Hu H-Y (2018) PolyQ-expanded huntingtin and ataxin-3 sequester ubiquitin adaptors hHR23B and UBQLN2 into aggregates via conjugated ubiquitin. *FASEB J* 32(6):2923–2933. <https://doi.org/10.1096/fj.20170801RR>
- Gerson JE, Safren N, Fischer S, Patel R, Crowley EV, Welday JP et al (2020) Ubiquilin-2 differentially regulates polyglutamine disease proteins. *Hum Mol Genet*. <https://doi.org/10.1093/hmg/ddaa152>
- Deng HX, Chen W, Hong ST, Boycott KM, Gorrie GH, Siddique N et al (2011) Mutations in UBQLN2 cause dominant X-linked juvenile and adult-onset ALS and ALS/dementia. *Nature* 477(7363):211–215. <https://doi.org/10.1038/nature10353>
- Le NT, Chang L, Kovlyagina I, Georgiou P, Safren N, Braunstein KE et al (2016) Motor neuron disease, TDP-43 pathology, and memory deficits in mice expressing ALS-FTD-linked UBQLN2 mutations. *Proc Natl Acad Sci USA* 113(47):E7580–E7589. <https://doi.org/10.1073/pnas.1608432113>
- Picher-Martel V, Renaud L, Bareil C, Julien JP (2019) Neuronal expression of UBQLN2(P497H) exacerbates TDP-43 pathology in TDP-43(G348C) mice through interaction with ubiquitin. *Mol Neurobiol* 56(7):4680–4696. <https://doi.org/10.1007/s12035-018-1411-3>
- Hjerpe R, Bett JS, Keuss MJ, Solovyova A, McWilliams TG, Johnson C et al (2016) UBQLN2 mediates autophagy-independent protein aggregate clearance by the proteasome. *Cell* 166(4):935–949. <https://doi.org/10.1016/j.cell.2016.07.001>
- Itakura E, Zavodszky E, Shao S, Wohlever ML, Keenan RJ, Hegde RS (2016) Ubiquilins chaperone and triage mitochondrial membrane proteins for degradation. *Mol Cell* 63(1):21–33. <https://doi.org/10.1016/j.molcel.2016.05.020>
- Chen T, Huang B, Shi X, Gao L, Huang C (2018) Mutant UBQLN2(P497H) in motor neurons leads to ALS-like phenotypes and defective autophagy in rats. *Acta Neuropathol Commun* 6(1):122. <https://doi.org/10.1186/s40478-018-0627-9>
- Sharkey LM, Sandoval-Pistorius SS, Moore SJ, Gerson JE, Komlo R, Fischer S et al (2020) Modeling UBQLN2-mediated neurodegenerative disease in mice: shared and divergent properties of wild type and mutant UBQLN2 in phase separation, subcellular localization, altered proteostasis pathways, and selective cytotoxicity. *Neurobiol Dis*. <https://doi.org/10.1016/j.nbd.2020.105016>
- Chang L, Monteiro MJ (2015) Defective proteasome delivery of polyubiquitinated proteins by ubiquilin-2 proteins containing ALS mutations. *PLoS ONE* 10(6):e0130162. <https://doi.org/10.1371/journal.pone.0130162>
- Osaka M, Ito D, Suzuki N (2016) Disturbance of proteasomal and autophagic protein degradation pathways by amyotrophic lateral sclerosis-linked mutations in ubiquilin 2. *Biochem Biophys Res Commun* 472(2):324–331. <https://doi.org/10.1016/j.bbrc.2016.02.107>
- Sharkey LM, Safren N, Pithadia AS, Gerson JE, Dulchavsky M, Fischer S et al (2018) Mutant UBQLN2 promotes toxicity by modulating intrinsic self-assembly. *Proc Natl Acad Sci* 115(44):E10495–E10504. <https://doi.org/10.1073/pnas.1810522115>
- Halloran M, Ragagnin AMG, Vidal M, Parakh S, Yang S, Heng B et al (2019) Amyotrophic lateral sclerosis-linked UBQLN2 mutants inhibit endoplasmic reticulum to Golgi transport, leading to Golgi fragmentation and ER stress. *Cell Mol Life Sci*. <https://doi.org/10.1007/s00018-019-03394-w>
- Wu JJ, Cai A, Greenslade JE, Higgins NR, Fan C, Le NTT et al (2020) ALS/FTD mutations in UBQLN2 impede autophagy by reducing autophagosome acidification through loss of function. *Proc Natl Acad Sci*. <https://doi.org/10.1073/pnas.1917371117>
- Rutherford NJ, Lewis J, Clippinger AK, Thomas MA, Adamson J, Cruz PE et al (2013) Unbiased screen reveals ubiquilin-1 and -2

- highly associated with huntingtin inclusions. *Brain Res* 1524:62–73. <https://doi.org/10.1016/j.brainres.2013.06.006>
29. Frottin F, Schueder F, Tiwary S, Gupta R, Korner R, Schlichthaerle T et al (2019) The nucleolus functions as a phase-separated protein quality control compartment. *Science* 365(6451):342–347. <https://doi.org/10.1126/science.aaw9157>
  30. Mediani L, Guillén-Boixet J, Vinet J, Franzmann TM, Bigi I, Mateju D et al (2019) Defective ribosomal products challenge nuclear function by impairing nuclear condensate dynamics and immobilizing ubiquitin. *EMBO J* 38(15):e101341. <https://doi.org/10.15252/emboj.2018101341>
  31. Latonen L, Moore HM, Bai B, Jäämaa S, Laiho M (2011) Proteasome inhibitors induce nucleolar aggregation of proteasome target proteins and polyadenylated RNA by altering ubiquitin availability. *Oncogene* 30(7):790–805. <https://doi.org/10.1038/onc.2010.469>
  32. Gallardo P, Real-Calderón P, Flor-Parra I, Salas-Pino S, Daga RR (2020) Acute heat stress leads to reversible aggregation of nuclear proteins into nucleolar rings in fission yeast. *Cell Rep*. <https://doi.org/10.1016/j.celrep.2020.108377>
  33. Frattini A, Faranda S, Zucchi I, Vezzoni P (1997) A low-copy repeat in Xq26 represents a novel putatively prenylated protein gene (CXX1) and its pseudogenes (DXS9914, DXS9915, and DXS9916). *Genomics* 46(1):167–169. <https://doi.org/10.1006/geno.1997.5006>
  34. Brandt J, Veith AM, Volff JN (2005) A family of neofunctionalized Ty3/gypsy retrotransposon genes in mammalian genomes. *Cytogenet Genome Res* 110(1–4):307–317. <https://doi.org/10.1159/000084963>
  35. Boot A, Oosting J, van Eendenburg JDH, Kuppen PJK, Morreau H, van Wezel T (2017) Methylation associated transcriptional repression of ELOVL5 in novel colorectal cancer cell lines. *PLoS ONE* 12(9):e0184900. <https://doi.org/10.1371/journal.pone.0184900>
  36. Whiteley AM, Prado MA, de Poot SAH, Paulo JA, Ashton M, Dominguez S et al (2020) Global proteomics of Ubqln2-based murine models of ALS. *J Biol Chem*. <https://doi.org/10.1074/jbc.RA120.015960>
  37. Zheng W, Li Y, Zhang C, Pearce R, Mortuza SM, Zhang Y (2019) Deep-learning contact-map guided protein structure prediction in CASP13. *Proteins* 87(12):1149–1164. <https://doi.org/10.1002/prot.25792>
  38. Zhang C, Lane L, Omenn GS, Zhang Y (2019) Blinded testing of function annotation for uPE1 proteins by I-TASSER/COFAC-TOR pipeline using the 2018–2019 additions to neXtProt and the CAFA3 challenge. *J Proteome Res* 18(12):4154–4166
  39. Xu J, Zhang Y (2010) How significant is a protein structure similarity with TM-score = 0.5? *Bioinformatics* 26(7):889–895
  40. Ashley J, Cordy B, Lucia D, Fradkin LG, Budnik V, Thomson T (2018) Retrovirus-like Gag protein Arc1 binds RNA and traffics across synaptic boutons. *Cell* 172(1–2):262–74.e11. <https://doi.org/10.1016/j.cell.2017.12.022>
  41. Klima JC, Doyle LA, Lee JD, Rappleye M, Gagnon LA, Lee MY et al (2021) Incorporation of sensing modalities into de novo designed fluorescence-activating proteins. *Nat Commun* 12(1):856. <https://doi.org/10.1038/s41467-020-18911-w>
  42. Feric M, Vaidya N, Harmon TS, Mitrea DM, Zhu L, Richardson TM et al (2016) Coexisting liquid phases underlie nucleolar subcompartments. *Cell* 165(7):1686–1697. <https://doi.org/10.1016/j.cell.2016.04.047>
  43. Welch WJ, Feramisco JR (1984) Nuclear and nucleolar localization of the 72,000-dalton heat shock protein in heat-shocked mammalian cells. *J Biol Chem* 259(7):4501–4513
  44. Lewis MJ, Pelham HR (1985) Involvement of ATP in the nuclear and nucleolar functions of the 70 kD heat shock protein. *Embo J* 4(12):3137–3143
  45. Pankiv S, Lamark T, Bruun J-A, Øvervatn A, Bjørkøy G, Johansen T (2010) Nucleocytoplasmic shuttling of p62/SQSTM1 and its role in recruitment of nuclear polyubiquitinated proteins to promyelocytic leukemia bodies. *J Biol Chem* 285(8):5941–5953. <https://doi.org/10.1074/jbc.M109.039925>
  46. Pikkariainen M, Hartikainen P, Soinen H, Alafuzoff I (2011) Distribution and pattern of pathology in subjects with familial or sporadic late-onset cerebellar ataxia as assessed by p62/sequestosome immunohistochemistry. *Cerebellum* 10(4):720–731. <https://doi.org/10.1007/s12311-011-0281-2>
  47. Baloh RH (2011) TDP-43: the relationship between protein aggregation and neurodegeneration in amyotrophic lateral sclerosis and frontotemporal lobar degeneration. *FEBS J* 278(19):3539–3549. <https://doi.org/10.1111/j.1742-4658.2011.08256.x>
  48. Udan-Johns M, Bengoechea R, Bell S, Shao J, Diamond MI, True HL et al (2014) Prion-like nuclear aggregation of TDP-43 during heat shock is regulated by HSP40/70 chaperones. *Hum Mol Genet* 23(1):157–170. <https://doi.org/10.1093/hmg/ddt408>
  49. Kang Y, Zhang N, Koepp DM, Walters KJ (2007) Ubiquitin receptor proteins hHR23a and hPLIC2 interact. *J Mol Biol* 365(4):1093–1101. <https://doi.org/10.1016/j.jmb.2006.10.056>
  50. Marín I (2014) The ubiquilin gene family: evolutionary patterns and functional insights. *BMC Evol Biol* 14(1):63. <https://doi.org/10.1186/1471-2148-14-63>
  51. Zheng T, Yang Y, Castaneda CA (2020) Structure, dynamics and functions of UBQLNs: at the crossroads of protein quality control machinery. *Biochem J* 477(18):3471–3497. <https://doi.org/10.1042/BCJ20190497>
  52. Samant RS, Livingston CM, Sontag EM, Frydman J (2018) Distinct proteostasis circuits cooperate in nuclear and cytoplasmic protein quality control. *Nature* 563(7731):407–411. <https://doi.org/10.1038/s41586-018-0678-x>
  53. Jachimowicz RD, Beleggia F, Isensee J, Velpula BB, Goergens J, Bustos MA et al (2019) UBQLN4 represses homologous recombination and is overexpressed in aggressive tumors. *Cell* 176(3):505–19.e22. <https://doi.org/10.1016/j.cell.2018.11.024>
  54. Carmo-Fonseca M, Mendes-Souares L, Campos I (2000) To be or not to be in the nucleolus. *Nat Cell Biol* 2(6):E107–E112. <https://doi.org/10.1038/35014078>
  55. Boisvert F-M, van Koningsbruggen S, Navascués J, Lamond AI (2007) The multifunctional nucleolus. *Nat Rev Mol Cell Biol* 8(7):574–585. <https://doi.org/10.1038/nrm2184>
  56. Latonen L (2019) Phase-to-phase with nucleoli—stress responses, protein aggregation and novel roles of RNA. *Front Cell Neurosci*. <https://doi.org/10.3389/fncel.2019.00151>
  57. Hernandez-Verdun D (2006) The nucleolus: a model for the organization of nuclear functions. *Histochem Cell Biol* 126(2):135. <https://doi.org/10.1007/s00418-006-0212-3>
  58. Fu A, Cohen-Kaplan V, Avni N, Livneh I, Ciechanover A (2021) p62-containing, proteolytically active nuclear condensates, increase the efficiency of the ubiquitin–proteasome system. *Proc Natl Acad Sci* 118(33):e2107321118. <https://doi.org/10.1073/pnas.2107321118>
  59. Zheng T, Galagedera SKK, Castañeda CA (2021) Previously uncharacterized interactions between the folded and intrinsically disordered domains impart asymmetric effects on UBQLN2 phase separation. *Protein Sci* 30(7):1467–1481. <https://doi.org/10.1002/pro.4128>
  60. Dao TP, Martyniak B, Canning AJ, Lei Y, Colicino EG, Cosgrove MS et al (2019) ALS-linked mutations affect UBQLN2 oligomerization and phase separation in a position- and amino acid-dependent manner. *Structure* 27(6):937–51.e5. <https://doi.org/10.1016/j.str.2019.03.012>
  61. Gerson JE, Linton H, Xing J, Sutter AB, Kakos FS, Ryou J et al (2021) Shared and divergent phase separation and aggregation

- properties of brain-expressed ubiquilins. *Sci Rep* 11(1):287. <https://doi.org/10.1038/s41598-020-78775-4>
62. Paolantoni C, Ricciardi S, De Paolis V, Okenwa C, Catalanotto C, Ciotti MT et al (2018) Arc 3' UTR splicing leads to dual and antagonistic effects in fine-tuning arc expression upon BDNF signaling. *Front Mol Neurosci* 11:145. <https://doi.org/10.3389/fnmol.2018.00145>
63. Moran DM, Shen H, Maki CG (2009) Puromycin-based vectors promote a ROS-dependent recruitment of PML to nuclear inclusions enriched with HSP70 and proteasomes. *BMC Cell Biol* 10:32. <https://doi.org/10.1186/1471-2121-10-32>
64. Guo L, Giasson BI, Glavis-Bloom A, Brewer MD, Shorter J, Gitler AD et al (2014) A cellular system that degrades misfolded proteins and protects against neurodegeneration. *Mol Cell* 55(1):15–30. <https://doi.org/10.1016/j.molcel.2014.04.030>
65. Lamoliatte F, McManus FP, Maarifi G, Chelbi-Alix MK, Thibault P (2017) Uncovering the SUMOylation and ubiquitylation crosstalk in human cells using sequential peptide immunopurification. *Nat Commun* 8:14109. <https://doi.org/10.1038/ncomms14109>
66. Rott R, Szargel R, Shani V, Hamza H, Savyon M, Abd Elghani F et al (2017) SUMOylation and ubiquitination reciprocally regulate  $\alpha$ -synuclein degradation and pathological aggregation. *Proc Natl Acad Sci USA* 114(50):13176–13181. <https://doi.org/10.1073/pnas.1704351114>
67. Jin J (2019) Interplay between ubiquitylation and SUMOylation: empowered by phase separation. *J Biol Chem* 294(42):15235–15236. <https://doi.org/10.1074/jbc.H119.011037>
68. Pankiv S, Lamark T, Bruun JA, Overvatn A, Bjorkoy G, Johansen T (2010) Nucleocytoplasmic shuttling of p62/SQSTM1 and its role in recruitment of nuclear polyubiquitinated proteins to promyelocytic leukemia bodies. *J Biol Chem* 285(8):5941–5953. <https://doi.org/10.1074/jbc.M109.039925>
69. Beauclair G, Bridier-Nahmias A, Zagury J-F, Saïb A, Zamborlini A (2015) JASSA: a comprehensive tool for prediction of SUMOylation sites and SIMs. *Bioinformatics* 31(21):3483–3491. <https://doi.org/10.1093/bioinformatics/btv403>
70. Flores BN, Li X, Malik AM, Martinez J, Beg AA, Barmada SJ (2019) An intramolecular salt bridge linking TDP43 RNA binding, protein stability, and TDP43-dependent neurodegeneration. *Cell Rep* 27(4):1133–50.e8. <https://doi.org/10.1016/j.celrep.2019.03.093>
71. Seyfried NT, Gozal YM, Dammer EB, Xia Q, Duong DM, Cheng D et al (2010) Multiplex SILAC analysis of a cellular TDP-43 proteinopathy model reveals protein inclusions associated with SUMOylation and diverse polyubiquitin chains. *Mol Cell Proteomics* 9(4):705–718. <https://doi.org/10.1074/mcp.M800390-MCP200>
72. Dangoumau A, Veyrat-Durebex C, Blasco H, Praline J, Corcia P, Andres CR et al (2013) Protein SUMOylation, an emerging pathway in amyotrophic lateral sclerosis. *Int J Neurosci* 123(6):366–374. <https://doi.org/10.3109/00207454.2012.761984>
73. Zybailov B, Mosley AL, Sardiu ME, Coleman MK, Florens L, Washburn MP (2006) Statistical analysis of membrane proteome expression changes in *Saccharomyces cerevisiae*. *J Proteome Res* 5(9):2339–2347. <https://doi.org/10.1021/pr060161n>
74. Wickham H (2009) ggplot2: elegant graphics for data analysis. *Use R*. <https://doi.org/10.1007/978-0-387-98141-3>
75. Kleijnen MF, Shih AH, Zhou P, Kumar S, Soccio RE, Kedersha NL et al (2000) The hPLIC proteins may provide a link between the ubiquitination machinery and the proteasome. *Mol Cell* 6(2):409–419. [https://doi.org/10.1016/S1097-2765\(00\)00040-X](https://doi.org/10.1016/S1097-2765(00)00040-X)
76. Lim J, Hao T, Shaw C, Patel AJ, Szabó G, Rual J-F et al (2006) A protein–protein interaction network for human inherited ataxias and disorders of purkinje cell degeneration. *Cell* 125(4):801–814. <https://doi.org/10.1016/j.cell.2006.03.032>
77. Bolte S, Cordelières FP (2006) A guided tour into subcellular colocalization analysis in light microscopy. *J Microsc* 224(Pt 3):213–232. <https://doi.org/10.1111/j.1365-2818.2006.01706.x>
78. Carpenter AE, Jones TR, Lamprecht MR, Clarke C, Kang IH, Friman O et al (2006) Cell Profiler: image analysis software for identifying and quantifying cell phenotypes. *Genome Biol* 7(10):R100. <https://doi.org/10.1186/gb-2006-7-10-r100>
79. Robert X, Gouet P (2014) Deciphering key features in protein structures with the new ENDscript server. *Nucleic Acids Res* 42(W1):W320–W324. <https://doi.org/10.1093/nar/gku316>

**Publisher's Note** Springer Nature remains neutral with regard to jurisdictional claims in published maps and institutional affiliations.